1960

Effect of radiation on the electrical conductivity in bismuth

Donald Duane Glower
Iowa State University

Mic 61-448

GLOWER, Donald Duane. EFFECT OF RADIATION ON THE ELECTRICAL CONDUCTIVITY IN BISMUTH.

Iowa State University of Science and Technology
Ph.D., 1960
Physics, solid state

University Microfilms, Inc., Ann Arbor, Michigan

EFFECT OF RADIATION ON THE ELECTRICAL CONDUCTIVITY IN BISMUTH

by

Donald Duane Glower

A Dissertation Submitted to the
Graduate Faculty in Partial Fulfillment of
The Requirements for the Degree of
DOCTOR OF PHILOSOPHY

Major Subject: Nuclear Engineering

Approved:

Signature was redacted for privacy.

In Charge of Major Work

Signature was redacted for privacy.

Head of Major Department

Signature was redacted for privacy.

Dean of Graduate College

Iowa State University
Of Science and Technology
Ames, Iowa

1960

TABLE OF CONTENTS

I. INTRODUCTION

A. Purpose of the Experiment

The theory of radiation effects in solids is in its infancy. Current theories are being tested experimentally as rapidly as the development of experimental techniques allows. The intent of this thesis is to add to the knowledge of the physical properties of bismuth, to introduce and to apply a technique which will gain additional information from existing data, and to provide a means of correlation between theory and experiment.

Shortly after nuclear reactors provided researchers with a neutron flux of a high order of magnitude, as cited in Seitz (1), E. P. Wigner suggested that such concentrations could possibly damage solids and alter their physical properties. A study of possible radiation effects was then made, and the theory of radiation effects began to emerge. Researchers began publishing results concerning radiation effects on the physical properties of a great variety of materials. These data were published without knowledge of the neutron and gamma flux spectra in the vicinity of the experiment, without statement of the impurity concentrations in the material, without determination of the crystal size, and, in some cases, without reference to the temperature variation and control. Because of this and the fact that

these materials were irradiated in many different reactors with different means of signifying radiation amounts and with no special consideration given to the saturation point, which is dependent upon the magnitude of the flux, it is understandable that much of the present data appears inconsistent.

Reliable data are available today through research done with instruments which provide monoenergetic particles. However, such particle sources normally do not have the high flux levels which are available from nuclear reactors. There is a need for an accurate method of determining the neutron and gamma flux spectra at the test specimen within a reactor before the nuclear reactor can fulfill the original expectations for its use as a research tool. When the neutron and gamma flux spectra at the test specimen have been determined, the irradiation data from the various reactors can be more realistically compared.

A new foil technique is being developed which will determine the neutron flux spectra at the irradiation site. This foil technique was used to determine an approximate spectra which was then used in the theoretical calculations for estimating the magnitude of the production rate of various irradiation effects.

Each type of radiation effect has an energy threshold for formation as well as an activation energy for annealing. This difference in annealing activation energy suggests that

the effects will decay out at different rates. The experimental procedure is to monitor the electrical resistivity change during annealing, and then plot the data on semilog paper. When this is done in the manner used for radioactive decay processes, it is seen that distinct half lives are present revealing the relative effect of each type of process upon the electrical resistivity.

This procedure is contrasted with that normally used where the temperature is raised at a controlled rate. Both methods reveal certain thresholds. However, the technique used in this experiment appears to give a more distinct picture of the individual processes influencing the magnitude of the electrical resistance.

B. Known Properties of Bismuth

Bismuth is a brittle semi-metal which is usually described as tin white in color but with a distinct reddish tinge and a high luster. It is the third member of the arsenic, antimony, bismuth subgroup of the fifth group of the periodic table. Bismuth has the highest density of the three members of its subgroup. It has the atomic number 83, the next in order above lead, and an atomic weight of 209. The bismuth lattice can be described in two ways, either as a lattice in which the rhombohedral angle is nearly 90^{o}, the unit cell containing eight atoms, or as a rhombohedral lattice with an angle which is $57^{o}\ 16'$, the unit cell

containing two atoms. The atoms are arranged in double layers, each atom having three nearest neighbors at a distance 3.11 angstroms and three next nearest neighbors at the greater distance of 3.47 angstroms. The lattice constant a is 4.74 angstroms.

The density of bismuth is 9.8 grams per cm^3 at 20^o C and 10.067 grams per cm^3 at its melting point of 277^o C. The expansion of the metal during solidification amounts to 3.32 percent of its volume at its melting point.

Bismuth has a valence of five. These five electrons are capable of filling a Brillouin zone. However, it is held that the comparative smallness of the energy discontinuities at the zone boundaries allows some of the electrons to overlap into the next zone, leaving a number of holes in the almost filled band. Quantitative calculations of the energy discontinuities are lacking since the precise band structure of bismuth is not known. The number of electrons which are free is so small that it can be altered appreciably by the addition of suitable impurities. When small quantities of selenium are added to bismuth, the resistivity initially drops and then increases with a steep curve as the impurity concentration nears one percent. An impurity such as lead or tin causes the resistivity to increase with a very sharp curve initially, and then to flatten out between one and two percent impurity concentration.

Wilson (2) has analyzed the effect of impurities on single bismuth crystals in the following manner. When lead is added as an impurity, there is a certain concentration that will cause a maximum in the resistivity versus temperature curve. Lead has fewer valency electrons than bismuth. Thus, when lead is added as the impurity it reduces the number of electrons in the upper Brillouin zone. A sufficient amount of lead will eliminate the number of electrons in the upper Brillouin zone, but will leave some vacant levels in the lower zone. This alloy behaves normally at low temperature, but at higher temperature electrons are excited into the upper zone, thereby decreasing the resistivity. Experiments on single crystals to which the lead impurity was added demonstrated that 0.1 percent of lead is sufficient to produce a maximum in $\rho_{\parallel}$ while one percent is required to produce a maximum in $\rho_{\perp}$. This means that approximately 0.7 percent lead impurity would be required to produce the maximum in polysrystalline bismuth.

On the other hand, selenium has more than five valency electrons. Thus, the extra electrons go into the upper zone increasing the conductivity. As more selenium is added, the holes again fill and the conductivity decreases.

II. LITERATURE REVIEW

The literature covers almost all phases of radiation effects in materials. Practically all materials, including many alloys of metals, have been subjected to some form of radiation study. However, as mentioned previously, the amount of this mass of information that has been gathered under controlled or known conditions is very small. Since there is such a hugh accumulation of information, a number of very good review articles are available.

References (1), (3), and (4) cover the period through 1957. Almost all the important publications are listed in these works. Reference (1) is an article which covers quite thoroughly the theory and the experimental work which took place before 1956. The fourth reference is a text that carries the theory on through 1957. This book consists of six chapters dealing with the various aspects of radiation effects in solids, and lists as many as 120 references, papers and books, at the end of each chapter. The period from 1957 to date has been covered in an article by Brooks (5).

The present interpretation of the changes in the properties of solids brought about by high energy radiation centers about the production of several types of defects in the solid. These defects are vacancies, interstitial atoms, and impurity atoms. In addition to these defects there are replacement collisions, thermal and displacement spikes, and ionization

effects.

The formal theory of displacement production was first published in 1948 by Bohr (6) in the classified literature. Seitz and others pursued the theory in the unclassified literature for the next several years. Several models for displacement and interstitial formation were proposed. Then, in 1955, two mathematical models were presented which are today considered to be probably near the correct answer. The first was by Snyder and Neufeld (7) who gave a mathematical procedure for determining the number of vacant lattice sites or interstitial atoms in a monoatomic solid. This model followed the formal treatment of Bohr, and presented a solution obtained after utilizing many complex mathematical theories. The second model was presented by Kinchin and Pease (3). The fundamental difference between the two models is that the Kinchin and Pease model assumes that a struck atom is not required to climb out of a potential well before being in a position to make displacing collisions with other atoms. On the other hand, Snyder and Neufeld assume that the atom loses energy E_d before moving off through the lattice to make other displacements. The Kinchin and Pease model also differs by taking into consideration the possibility that an incoming atom may be captured in the lattice site from which the knock-on atom was displaced. Both models give results which are nearly identical. More complex models (1) do not produce

significant differences in the end result.

All present models include an assumption concerning the energy E_d required for displacement. Huntington (8) has employed the best approximation method presently available to estimate the displacement energy. The results indicated the possibility of several types of displacement energies depending upon the direction in which the knock-on atom moves. The range of energy lies between 18.5 and 43 electron volts for copper. Seitz (9) had previously calculated a theoretical expression which Huntington utilized in his approximation method. Seitz had suggested 25 ev as a good approximation for E_d for most materials. Huntington's calculation tends to verify Seitz's assumption, at least so far as copper is concerned. Therefore, it appears that the value suggested by Seitz is the best currently available. Most theoretical calculations use this value of displacement energy. The experimental work which has been done on a number of materials is reviewed by Dienes and Vineyard (4). The results, however, are not in complete agreement.

In 1954 Brinkman (10) proposed a model for radiation damage in metals. He suggests that there are thermal and displacement spikes caused by neutron irradiation. Previously temperature spikes which are comparable to the thermal spike of Brinkman were presented. The two mathematical models discussed by the author cover the thermal spike of Brinkman.

However, the authors of the mathematical models did not pay particular attention to the primary knock-on atom after its energy became too low to cause further displacements. Brinkman follows this primary knock-on atom through the thermal spike until its energy is below the displacement energy, and then assumes the remaining energy is transferred to the lattice bringing the lattice in the immediate vicinity to the molten state with considerable turbulent flow. He estimates that 10^4 or more atoms in a spherical region known as the displacement spike will be effected at the end of the thermal spike. This region will start freezing on the outside, and thus should solidify largely in orientation with the original crystal although some misoriented regions and entangled dislocation loops will remain. This is the model which is generally accepted today.

The literature reveals that many experiments are concerned with the production rate of the displacements. The procedure is to irradiate the specimen at low temperatures and to monitor the change in electrical resistivity. If the slope of the curve for change in resistivity versus time is constant, it can be assumed that the damage is not annealing out. Normally there is some annealing. Therefore, the slope at time $t = 0$ is considered the indication of the production rate. Several materials were irradiated at about 20° K (11) at Oak Ridge, and, although the slopes were different for

different materials, the slope for each material was constant.

Impurity atoms are formed under neutron bombardment by transmutation. This method of adding impurities has been utilized to assure a controlled rate of changing the impurity concentration. However, this is not considered to be important in bismuth since the absorption cross section is low.

The passage of charged particles or gamma rays through a solid may cause extensive ionization and electronic excitation which, in turn, lead to bond rupture, free radicals, coloration, luminescence, etc. in many types of solids. These effects are most important in the various insulators and dielectrics, ionic crystals, glasses, etc. Effects of this nature are reviewed in the text by Charlesby (12) as well as in references (1), (4), and (5).

Replacement collisions are important in polyatomic materials. This is reviewed in (1) and (3).

The annealing of defects has received considerable attention in the literature on radiation damage. Many of these articles are reviewed in references (1), (3), and (4). The theory and experiment tend to agree in predicting that the rate of annealing depends upon the type of imperfection, material involved, and temperature. It is generally agreed that there is an activation energy for each type of process.

The theory shows that this activation energy can be

evaluated in a number of different ways. Perhaps the most frequently employed method is to change the temperature suddenly, and then take a ratio of the two rate equations at the common point before and after the temperature change occurred. If, however, more than one type of imperfection is annealing at one time, this activation energy is a mean value for all processes.

The theory for annealing processes was initially developed using the technique of irradiating at low temperatures, and then theorizing as to the forms of impurities which were annealing at various temperatures. Current thinking in the field (5) tends to consider the annealing process as proceeding by the formation of groups of a specific defect type. Some of these groups are believed to migrate to the grain boundaries. Some data tend to support the proposal although nothing as yet is conclusive.

The final problem of concern in this thesis is the determination of a relationship between a specific type of defect and its relative effect on the electrical resistivity. Present day theory begins with the relationship presented by Mott and Jones in their text of 1936 (13). They present a relationship which gives the effect of impurity atoms on electrical resistivity. Several approaches are used by current investigators, (14) and (15), who are now interested in interstitials and in vacancies. The references cited here utilize

the work of several Ph.D. theses, (16) and (17), primarily from the University of Illinois. This work has been conducted on monovalent metals. The publication by Blatt (14) assumes the free electron approximation and Matthiessen's sum rule are valid. Blatt ignores relaxation of the lattice around the imperfections. With these and several other assumptions appropriate for the use of Hartree field and the partial wave method, he was able to set up suitable analytical relationships for solution on the ILLIAC computer. Thus, he determined the effects of the various impurities on the electrical resistivity of copper. Overhauser and Gorman made similar calculations for copper, but they used a different model. They employed the rigid ion model (2) as described by Wilson, and included relaxation of the lattice, but omitted the free electron approximation. Their results appear to be more in line with experimental data than those presented by Blatt. They find that the distortion of the lattice adds a significant amount to the resistivity.

III. THE THEORY

A. Discussion of Types of Irradiation (Reactor) Damage

The literature survey pointed out that certain types of irradiation may be more important in some types of material than in others. Since bismuth is a heavy element, it seems logical to assume that effects on the electrical resistivity from electron and gamma bombardment can be ignored when compared to the damage caused by the neutrons when the material is irradiated in a reactor. Therefore, only the effects resulting from neutron bombardment will be considered. This should give a good order of magnitude for the concentration of a specific type of defect.

For any particular type of damage caused by the neutrons, it is possible to write a rate equation which equates the rate of change in the number of impurities to the production rate minus the decay rate. This can be written in symbol form

$$\frac{dN}{dt} = P - \lambda N \qquad 1$$

where P equals the production rate, N is the number of impurities of a specific type, t is time, and λ is a decay constant that is dependent upon the particular type of process and the temperature.

The production rate depends upon the magnitude and energy spectra of the neutron flux as well as on the type of material

being bombarded. When the production of a certain type of damage is small compared to the original number of atoms available for damage, it is reasonable to assume that the production rate is constant and that the original number of target atoms also remains constant. Equation 1 then integrates into an equation showing that an equilibrium point is reached at which point the annealing rate equals the production rate. At this equilibrium point it is possible to write

$$P = \lambda N \quad . \qquad 2$$

Matthiessen's sum rule, when applied to the change in electrical resistivity at equilibrium, indicates that the total change in resistivity is equal to the sum of the changes caused by the individual types of damage. It can now be assumed that this change in resistivity attributed to a specific type of defect is proportional to the concentration of this type of defect, that is

$$\Delta \varrho = B N \quad . \qquad 3$$

When the reactor is shut down the production rate is zero and equation 1 becomes

$$\frac{dN}{dt} = - \lambda N \quad . \qquad 4$$

Substituting equation 3 into equation 4 results in

$$\frac{d(\Delta \varrho)}{dt} = -\lambda (\Delta \varrho) \quad . \qquad 5a$$

The literature has shown that the decay constant for interstitial and vacancy annealing is given by the relationship shown in equation 6,

$$\lambda = K e^{-E/kT} \quad . \qquad 6$$

Here K is a rate constant and E is the activation energy. The value for λ can be determined from the slope of the annealing curve. That is, equation 5a when integrated can be written as

$$\ln \frac{\Delta\rho - \Delta\rho_o}{\Delta\rho_{sat}} = -\lambda t \quad . \qquad 5b$$

In this equation $\Delta\rho_{sat}$ is the magnitude of the electrical resistivity which anneals, $\Delta\rho_o$ is the difference between the annealed equilibrium resistivity and the unirradiated resistivity and $\Delta\rho$ is the total change from the unirradiated resistivity. This indicates that if the production rate can be calculated theoretically and λ determined experimentally, the value for N, the number of interstitials, vacancies, or whatever the particular type of damage may be, can be determined. Once N is known, the proportionality constant between electrical resistivity due to that particular type defect and the concentration of that defect may be found from equation 3. The electrical resistivity due to a specific type defect can be determined from a graph of equation 5b. This is shown in section IV of this thesis.

B. Interstitial Atom and Vacant Lattice Site Pair Formation

A combination of the Snyder and Neufeld and Brinkman models of radiation damage will be used. The Snyder and Neufeld model will be applied to form the displacement pairs owing to the thermal spike and then the displacement spike

will be used as an additional means of forming interstitial and vacancy atoms as well as a form of permanent damage. Since the more complex mathematics do not produce a great change in this final result and the flux spectra and displacement energy are not known precisely, several simplifying assumptions will be made.

The total probability that a given atom will be displaced after a time t can be written

$$p = t \int \phi(E) \; G(E) \, dE \quad . \qquad 7$$

In this equation $\phi(E)$ is the neutron flux spectrum and G(E) is the probability that a given atom is displaced when a neutron of energy E is incident on unit area. This probability can be written

$$G(E) = \sigma_s \int_{E_d}^{T_m} g(T/E_d) \, \frac{dT}{T_m} \qquad 8$$

where it is assumed that the neutron scattering cross section is independent of energy and that isotropic scattering occurs. The differential scattering cross section included in equation 8 is

$$d\sigma = \frac{\sigma_s}{T_m} \, dT \quad . \qquad 9$$

In this relationship T_m represents the maximum energy that can be transferred from the neutron to the knock-on atom in one collision, that is

$$T_m = \frac{4A}{(1 + A)^2} \; E \sim \frac{4E}{A} \qquad 10$$

since $A >> 1$, ($A = M_2/M_1 \cong 209/1$) for bismuth. The function $g(T/E_d)$ is the number of secondaries produced by a primary knock-on atom. The relationship is derived by Snyder and Neufeld. It is

$$g_1(T/E_d) = 0.561\ (1 + T/E_d) \qquad T/E_d \geq 2.0 \qquad 11$$

$$g_2(T/E_d) = (1 + \ln T/E_d) \qquad 1 \leq T/E_d \leq 2\ . \qquad 12$$

Substituting into equation 8 and integrating results in

$$G_1(E) = \frac{0.561\ \sigma_s\ A}{4} \left[\ln \frac{T_m}{E_d} + \frac{T_m}{E_d} \right] \qquad 13$$

$$G_2(E) = \frac{A\ \sigma_s}{4} \left[\ln \frac{T_m}{E_d} + \frac{1}{2} (\ln \frac{T_m}{E_d})^2 \right] \ . \qquad 14$$

These can now be substituted into equation 7 as

$$p_1 = \frac{0.561\ t\ \sigma_s\ A}{4} \int_{50}^{10^7} \phi(E) \left[\ln T_m/E_d + T_m/E_d - 1 \right] dE \qquad 15$$

$$p_2 = \frac{A\ \sigma_s}{4} \int_{25}^{50} \phi(E) \left[\ln T_m/E_d + 1/2(\ln T_m/E_d)^2 \right] dE\ . \qquad 16$$

When these are integrated $p_1 >> p_2$ and the final result is

$$p = 5.21 \times 10^{-7}\ t \qquad 17$$

where t is in seconds. This result may not be more accurate than an order of magnitude due to the assumptions made in its derivation. Therefore, in bismuth where there are about

2.825×10^{22} atoms per cm^3, the production of interstitial atoms and vacant lattice site pairs is

$$P = 1.47 \times 10^{14} \text{ pairs per second.} \qquad 18$$

C. Comparison of the Effect of Interstitial Atoms and Vacant Lattice Sites on the Electrical Resistivity

It is possible to predict theoretically what effect interstitial atoms and vacant lattice sites will have on the electrical resistivity in monovalent metals. The theory as given by Mott and Jones (13) and Wilson (2) has been used in two recent publications (14), (15) concerned with copper. Many concepts which are in reasonable agreement with experimental data are used in these calculations. Such concepts are, for example, used in calculating the magnitude of the displacements of surrounding atoms caused by interstitials and vacancies as shown by Huntington (8). For his calculation he extended a theory given by Fuchs (18) and later revised by Seitz (19).

The present knowledge of the band structure of bismuth does not allow complete calculation. However, with a few assumptions it is possible to predict theoretically the relative importance of interstitial atoms when compared with the same number of vacant lattice sites.

In treating the interaction of the conduction electrons and the lattice distortion it is assumed that the motion of the electrons and the nuclei are independent to the first

order and that coupling between them is caused by the alteration in the potential energy due to the distortion.

Let $U(\vec{r} - \vec{R})$ be the effective potential energy of an electron arising from the atom located at the lattice point $\vec{R}$ of the crystal. Assume that the wave function of the electrons for the undistorted lattice will be Bloch waves

$$\psi_{\vec{k}} = \frac{u_{\vec{k}}\, e^{i\vec{k}\cdot\vec{r}}}{N^{1/2}} \quad . \qquad 19$$

When an atom is displaced from its normal position in the lattice, assuming that there is no deformation of the atom, the perturbing potential energy is

$$U(\vec{r} - \vec{R} - \vec{u}_g) - U(\vec{r} - \vec{R}) = \vec{u}_g \cdot \nabla U(\vec{r} - \vec{R}) \qquad 20$$

where $\vec{u}_g$ denotes the displacement of the lattice point $\vec{R}$. The total potential available for scattering is then

$$V = -\sum_g \vec{u}_g \cdot \nabla U(\vec{r} - \vec{R}) \quad . \qquad 21$$

In the zeroth approximation, the total wave function is the product of an electronic wave function and a lattice wave function. Since it has been assumed that each electron moves independently of the others, it is possible to concentrate upon one particular electron and discuss its possible transitions. To calculate the matrix element for the scattering of an electron from ψ_k to ψ'_k, it is necessary to evaluate the integral

$$V_{\vec{k}\vec{k}'} = \int \psi^*_{\vec{k}'} \sum_g e^{\pm i\vec{g}\cdot\vec{r}} \psi_{\vec{k}} \vec{u}_g \cdot \nabla U(\vec{r} - \vec{R})\, d\tau . \quad 22$$

Substituting equation 19 into equation 22 results in

$$V_{\vec{k}\vec{k}'} = -N^{-1} \int \vec{u}_g \cdot \nabla U(\vec{r} - \vec{R})\, e^{-i\vec{q}\cdot(\vec{r}-\vec{R})}\, u^*_{\vec{k}'}\, u_{\vec{k}}\, d\tau \quad 23$$

where $\vec{u}_k$ is normalized in the unit cell and the substitution $\vec{q} = \vec{k}' - \vec{k}$ is made. The integral can be approximately evaluated. The result is equal to $iC\vec{q}$ so that

$$V_{\vec{k}\vec{k}'} = -iCN^{-1} \sum_g \vec{q} \cdot \vec{u}_g\, e^{-i\vec{q}\cdot\vec{R}} \quad 24$$

where

$$C = \frac{\hbar^2}{3m} \int |\nabla u_{\vec{k}}|^2\, d\tau_o + \int V |u_{\vec{k}}|^2\, d\tau_o . \quad 25$$

This quantity C is the interaction constant between the electrons and the lattice, and is of the same order as the energy of the state $\vec{k}$ since the first term is two-thirds of the kinetic energy associated with $u_{\vec{k}}$, and the second is the mean potential energy. It will be considered constant.

The Born approximation (20) can be utilized if the scattering potential is not large. The differential scattering cross section can be shown to be

$$\sigma(\vec{k}_1, \vec{k}') = \frac{m^2 |V_{\vec{k}\vec{k}'}|^2}{4\pi^2 \hbar^4} = \zeta A \quad 26$$

where $\zeta = m^2 C^2 / 4\pi^2 N^2 \hbar^4$ 27

and $A = \left| \sum_g \vec{q} \cdot \vec{u}_g\, e^{-i\vec{q}\cdot\vec{R}} \right|^2$. 28

It is now necessary to calculate A for the set of lattice displacements $\vec{u}_g$ associated with an interstitial configuration. Huntington (8) has considered the elastic strains around an interstitial atom in copper. The configuration used had the interstitial located at the body centered position of the fcc cell. He chose the displacement of the atoms from their normal positions as follows:

$$\vec{u}_g = \epsilon \vec{R} \qquad \text{for nearest neighbors}$$

$$\vec{u}_g = \frac{g a^3 \vec{R}}{|R|^3} \qquad \text{for all other neighbors.} \qquad 29$$

The cell structure of bismuth is similar to that of copper, but somewhat distorted. The lattice vectors make an angle of $57^o\ 16'$ with each other. Therefore, it seems reasonable to choose displacements as indicated in $\vec{u}_g$. Overhauser and Gorman used the above relations for copper, and found that by comparison neighbors other than nearest neighbors had little influence. Therefore, this calculation will include only the influence of the nearest neighbors. An interstitial located in the center of the bismuth lattice will have two nearest neighbors at 2.24 angstroms, two neighbors at 2.40 angstroms, and two at 2.85 angstroms. It will be assumed that the overall effect approximates that of six atoms distributed over the surface of a sphere at a distance from the interstitial equal to the arithmetic mean value of their areas. This results in a distance equal to 2.57 angstroms.

It is difficult to evaluate the sum in equation 10

without approximation. Therefore, replacing the sum by an integral over the spherical surface results in

$$\left|\sum_g q \cdot u_g \, e^{-iq\cdot R^2}\right| \Rightarrow \left|\frac{6}{4\pi R^2}\int\int q \cdot R \, \text{Cox}\, \theta \, e^{iqR\,\text{Cos}\theta}\right.$$

$$\left. R^2 \,\text{Sin}\theta \, d\theta \, d\phi\right|^2 = \left| 6\epsilon \,\text{Cos}\, q\, R - \frac{1}{q\, R}\,\text{Sin}\, q\, R\right|^2 \quad , \qquad 30$$

in which $q = 2K_o \,\text{Sin}\, \theta/2$ where K_o is the wave number associated with the Fermi surface. The Fermi surface of bismuth is complex. However, assuming a spherical surface and using $E_F = 0.018$ ev, the wave number is $K_o = 0.155$ angstroms^{-1}. The relationship for the appropriate average cross section as given in Mott and Jones is

$$\sigma = \int \sigma \quad (\theta)\ (1 - \text{Cos}\ \theta)\ d\Omega \qquad . \qquad 31$$

Substituting equation 26 into equation 31 results in

$$\sigma = 496\,\pi\epsilon^2\,\zeta \qquad . \qquad 32$$

Mott and Jones give the following relationship for the resistivity caused by a one percent concentration of interstitial atoms:

$$\rho_o = \frac{\hbar\, K_o\, \sigma}{100\ e^2} \qquad . \qquad 33$$

The σ listed in equation 31 contains an electron-lattice interaction constant C and an effective electron mass m. These are difficult to evaluate. The effective mass in bismuth is not known with any precision. Therefore, the

technique used by Overhauser will eliminate this constant and mass and allow a direct comparison. The procedure is to write

$$\varrho_i = f\,\varrho_{exp} \qquad 34$$

where ϱ_i is the theoretical resistivity at low temperatures. This is in reasonable agreement with experiment, and is given by Wilson as

$$\varrho_i = \frac{3\pi m^2 C^2 T}{4\mu e^2 \hbar k \theta^2} \qquad 35$$

where

θ = Debye temperature, k = Boltzmann's constant,

μ = mass density, and T = absolute temperature.

The ϱ_{exp} in equation 34 is the resistivity without impurities measured at the temperature T. The factor f is the constant that takes into consideration the Umklapp contribution at higher temperatures. From equation 34, then, it is seen that

$$1 = \frac{f\,\varrho_{exp}}{\varrho_i} \quad , \qquad 36$$

and when this is multiplied by equation 33 there results

$$\varrho_o = f\,\frac{\hbar K_o \sigma\, \varrho_{exp}}{100\, e^2\, \varrho_i} \quad , \qquad 37a$$

or

$$\varrho_o = 496\, \epsilon^2 f \left(\frac{K_o \mu k \theta^2}{\hbar^2 \pi^2 300 N^2 T} \right) \varrho_{exp}. \qquad 37b$$

The value of the bracketed terms is 1.122. Therefore, the residual resistance due to one percent interstitial atoms is

$$\varrho_o = 556\, \epsilon^2 f\, \varrho_{exp} \quad . \qquad 38$$

An approach identical to that used above can be used for the vacant lattice site strain contribution to the resistivity. Bismuth has three nearest neighbors at 3.11 angstroms and the next three neighbors at 3.48 angstroms. Using arithmetic averages again, the mean distance is 3.29 angstroms. Using a δ in place of ϵ in the same type atomic displacement, only a negative displacement for vacancies, equation 37b appears as

$$\varrho_o = 104\, \delta^2 f\, \varrho_{exp} \quad . \qquad 39$$

It is necessary to add to the resistivity already given by 38 and 39 the contributions rising from the impurity itself, and the contribution from the interference between defect and strain scattering. This calculation was made by Jongenburger and Blatt employing a partial wave method and a solution on the ILLIAC computor. Their results indicated that the vacancy itself contributed approximately twice the value obtained from the vacancy strain scattering. The strain scattering for the interstitial accounts for 95 percent of the total resistivity attributed to this type of impurity.

If it is now assumed that the ratio of ϵ/δ is identical to that found by Huntington for copper and that equation 39

is only one-third the total value, the ratio becomes

$$\frac{\varrho_{int}}{\varrho_{vac}} = 4.5 \qquad 40$$

where ϵ/δ is taken to equal 1.6, the value for copper.

D. Production of Displacement Spikes

Displacement spikes are assumed to be produced by all neutrons having energies above E_d. If the equation for the flux is integrated the result indicates that there are approximately 2.28×10^{11} neutrons per cm^3 above this energy. This would then be the density of the displacement spikes. Brinkman believes that at least 10^4 atoms are involved in each displacement spike, and so this means approximately 2.28×10^{15} atoms/cm^3-sec are effected.

The model Brinkman proposed is difficult to present in mathematical form. It can be visualized that in a solid the displacement spike occurs as a molten sphere in which for a short time there is a high turbulent flow. This turbulent flow produces interstitial atoms along the surface of the sphere. When this sphere begins to solidify, it will do so initially along the outer periphery and proceed toward the center. Most solids will contract when cooled, thereby causing strains and dislocation loops. The center of the sphere will probably have a lower atomic density. The process leaves some of the atoms interstitially placed.

Bismuth may act somewhat differently. When the

dislocation spike is formed, the density increases with a volume decrease of about 3.3 percent. This means that there will be a lower than normal density surrounding the sphere. The turbulent flow involved in the sphere may be able to cause some of the atoms to assume deeper interstitial positions than would normally be true for other solids. Since the total number of atoms involved is of the same order of magnitude as the pair production, the displacement spike may provide a significant additional source of interstitial atoms. The primary effect, however, will be to introduce dislocation loops as it is reasonable to assume that the molten matter in the sphere will solidify in orientation with the crystal.

The dislocation loops will provide additional scattering centers for the conduction electrons and lattice waves. The theoretical calculation which would yield an estimate of the effect of a specific density of dislocations on the electrical resistivity must include the coupling between the conduction electrons and the lattice. This has not been adequately solved for comparatively simple metals such as copper. Therefore, the effect of dislocations in bismuth, where the electron lattice interaction is relatively large, will probably be significant.

E. Discussion of the Irradiation Effect by an Analysis of the Annealing Curve

The literature survey briefly mentioned the procedure

currently in use by many experimenters who are attempting to interpret the data which they collect. Annealing data can be analyzed in the same manner as the decay of a radioactive specimen containing several half lives. This technique is not suitable when more than three or four processes are present, or when processes in which the half lives are very near the same value are involved. However, for many radiation damage studies it appears to be very useful.

For example, the data as published by Overhauser (15) may be considered. In his paper and later in an analysis by Seitz (1), Overhauser states that there are probably two primary processes taking place and that the rate equation is of the form

$$\frac{d(\Delta \rho)}{dt} = K_o (\Delta \rho)^{\zeta} \qquad 41$$

where $\zeta = 2.5$. The magnitude of ζ indicates the complexity of the annealing process. Figure 1 shows a graph presented in Overhauser's publication. If the annealing is assumed to have reached equilibrium at $\Delta\rho_o = 0.24 \times 10^{-8}$ ohm-cm, then it is possible to plot the Figure 2 where $\Delta\rho_{sat}$ is the value of the total electrical resistivity which annealed. This plot appears to separate the two annealing processes clearly.

If this type of plot has separated two processes, it is possible to determine an activation energy and rate constant for each process. The slope of the curve in Figure 2 for each process can be equated to

Figure 1. Isothermal annealing curve for irradiated copper (-18.3° C) as published by Overhauser (15)

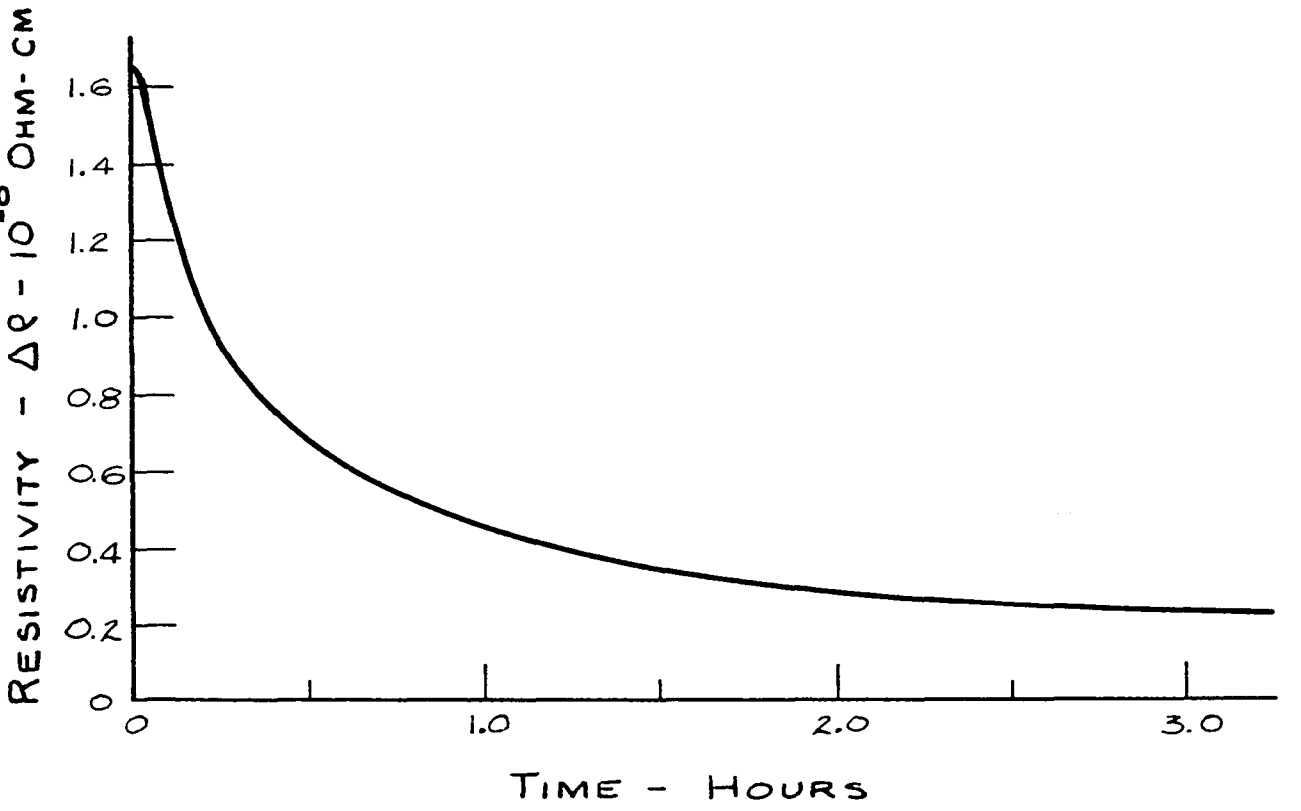
RESISTIVITY - Δρ - 10⁻⁸ OHM-CM
1.6
1.4
1.2
1.0
0.8
0.6
0.4
0.2
0
0
1.0
2.0
3.0
TIME - HOURS

Figure 2. Annealing data from Figure 1 replotted in a manner which reveals the half lives for two decay processes

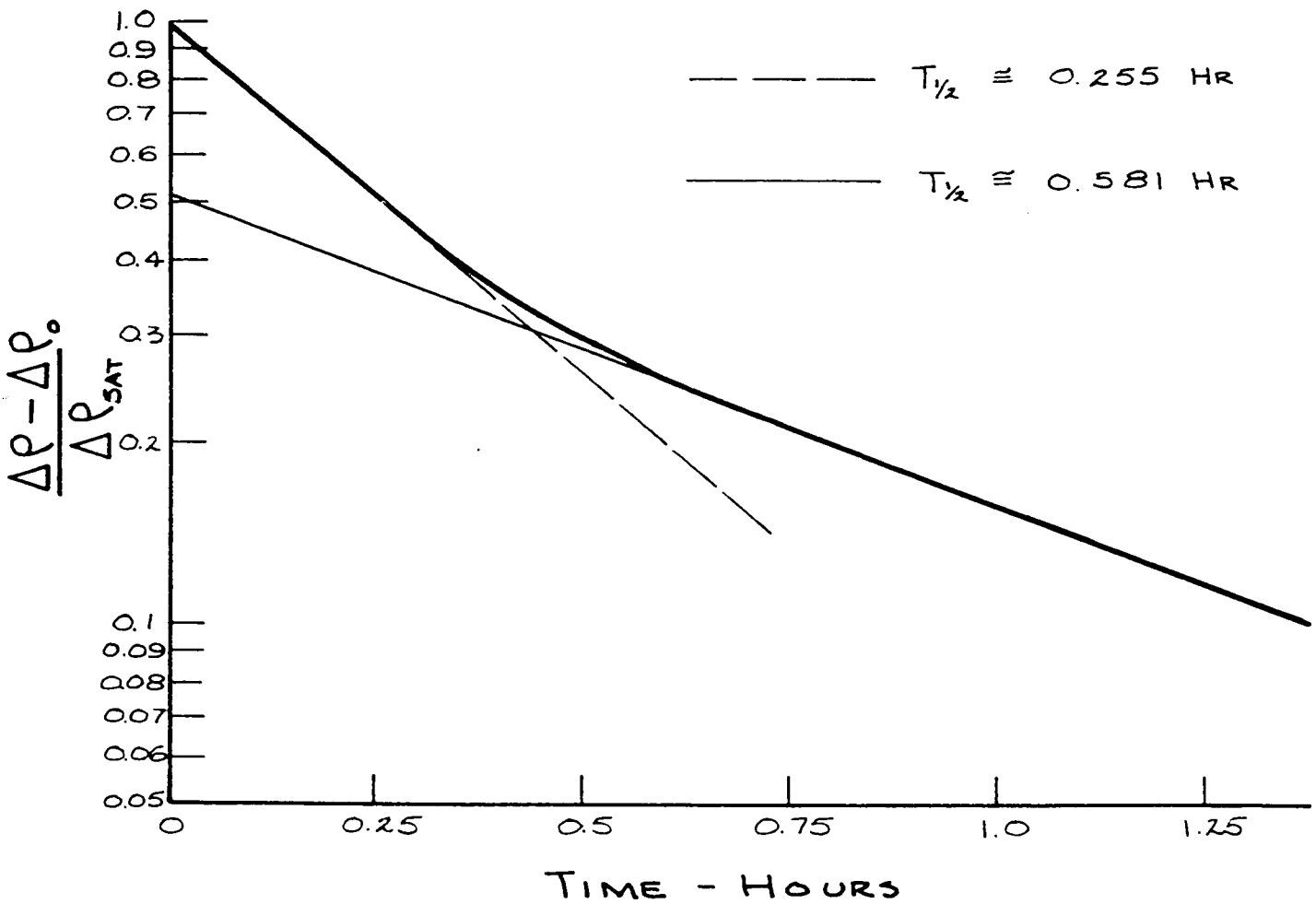
1.0
0.9
0.8
0.7
0.6
0.5
0.4
0.3
0.2
0.1
0.09
0.08
0.07
0.06
0.05
$\frac{\Delta P - \Delta P_0}{\Delta P_{SAT}}$
$T_{1/2} \cong 0.255$ HR
$T_{1/2} \cong 0.581$ HR
0
0.25
0.5
0.75
1.0
1.25
TIME - HOURS

$$\lambda = K_i \, e^{-E/kT} \qquad 42$$

where λ is determined experimentally for two different temperatures T. Simultaneous solution of the two relationships results in values for K_i and E.

Figure 2 is a graphical solution for the rate equations. The values of the resistivity at time zero can be interpreted to give the relative amount attributable to each process of the total resistivity which annealed. The ratio of this quantity can be compared with the theoretical estimate presented in equation 40.

IV. THE EXPERIMENT

A. Source of the Bismuth Crystals

The bismuth crystals were grown by Monocrystals Company, 1721 Sherwood Boulevard, Cleveland 17, Ohio, from material originally purchased from the American Smelting and Refining Company, South Plainfield, New Jersey. The latter states that for lot 60-2A the spectrographic analysis shows 99.999+ percent by difference pure bismuth.

B. Preparation of the Specimens

The polycrystalline specimen was prepared by Monocrystals Company so that the crystals were of approximately uniform size. The average grain size, determined by Monocrystals Company by direct comparison to the ASTM Grain Size Standards for the Estimation of the Diameters of Average Grain of Nonferrous Metals, was estimated at 1.1 mm in diameter, allowing for a slight elongation of the grain.

One purchased single crystal was one inch in diameter by one and one-half inches in length. The second single crystal, which contained some small surface crystals, was supplied in the dimension of one inch diameter by two and one-half inches in length to assure ample single crystal size. These two crystals were mounted in a Laue camera, and photographed in different orientations to locate the c axis.

The specimens were first cut with a Carborundum wheel

Figure 3. Contact locations in the Hall and magneto resistance measurements

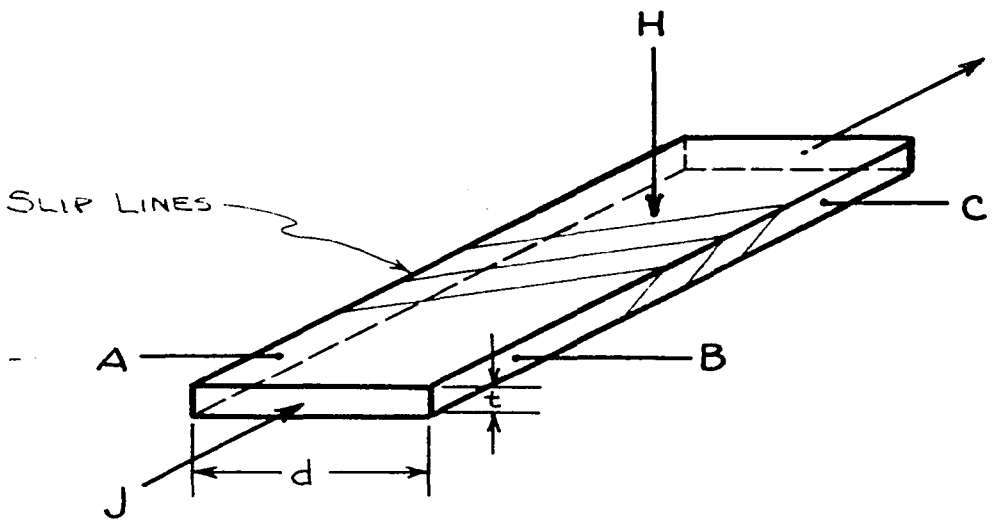
H
SLIP LINES
C
A
B
t
d
J

Figure 4. Magneto resistance of irradiated bismuth

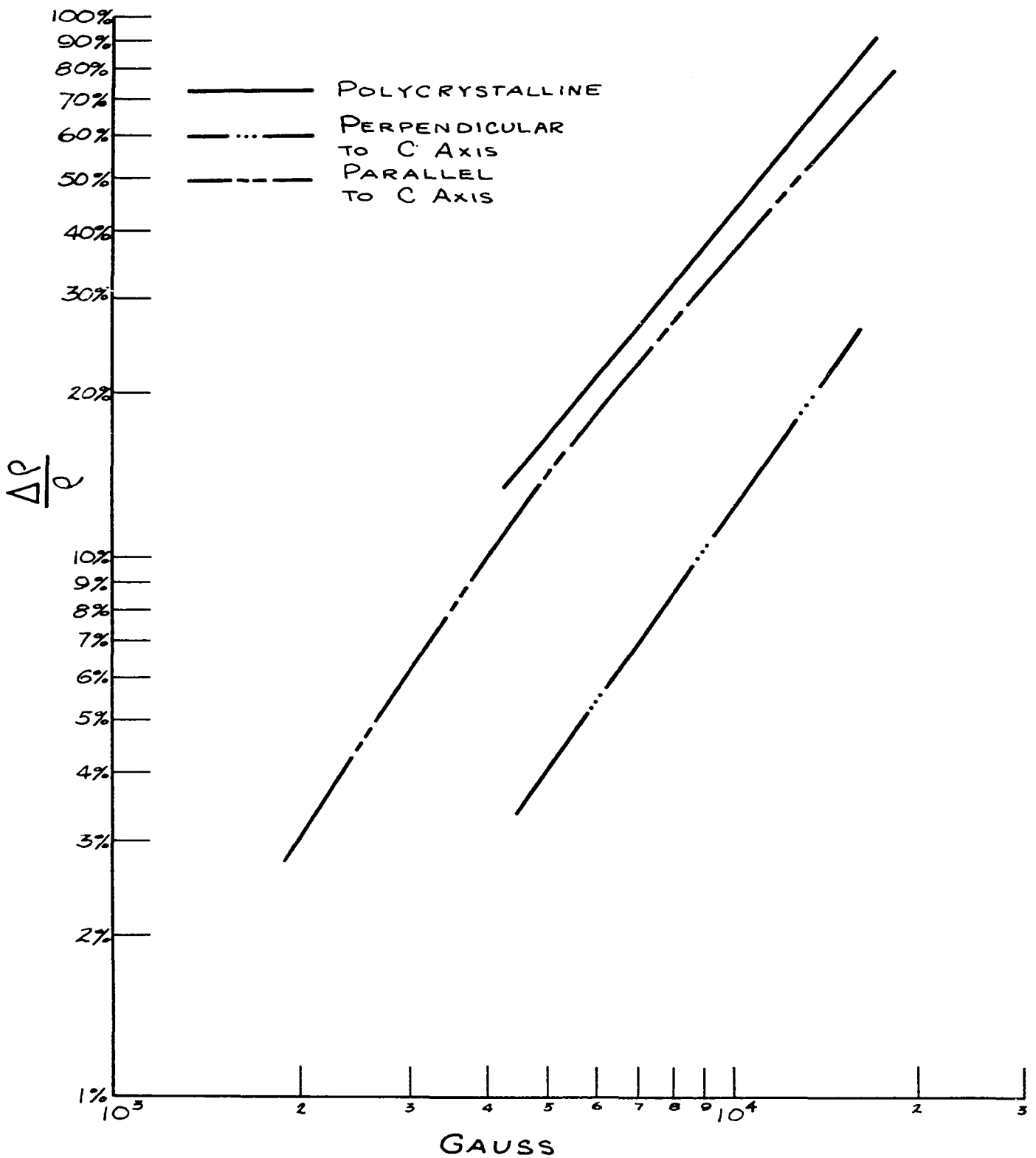
100%
90%
80%
70%
60%
50%
40%
30%
20%
10%
9%
8%
7%
6%
5%
4%
3%
2%
1%
Δρ/ρ
POLYCRYSTALLINE
PERPENDICULAR TO C AXIS
PARALLEL TO C AXIS
10³
2
3
4
5
6
7
8
9
10⁴
2
3
GAUSS

Figure 5. Hall coefficient data

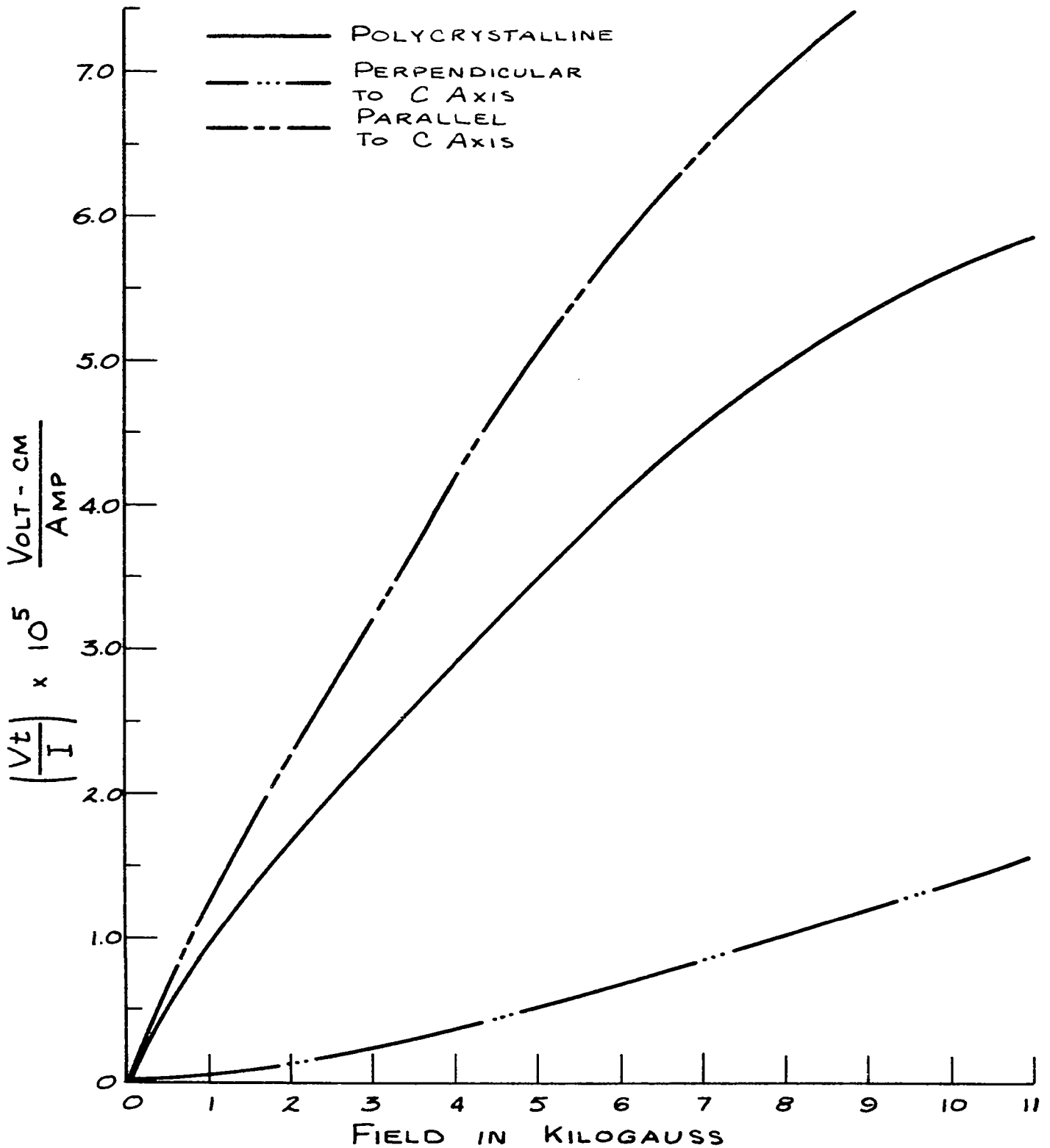
POLYCRYSTALLINE
PERPENDICULAR TO C AXIS
PARALLEL TO C AXIS
7.0
6.0
5.0
4.0
3.0
2.0
1.0
0
$\left(\frac{Vt}{I}\right) \times 10^5 \frac{\text{VOLT - CM}}{\text{AMP}}$
0 1 2 3 4 5 6 7 8 9 10 11
FIELD IN KILOGAUSS

Figure 6. Calculated Hall coefficients using $R_H = Vt/IH$ (evaluate at the intercept with the zero field axis)

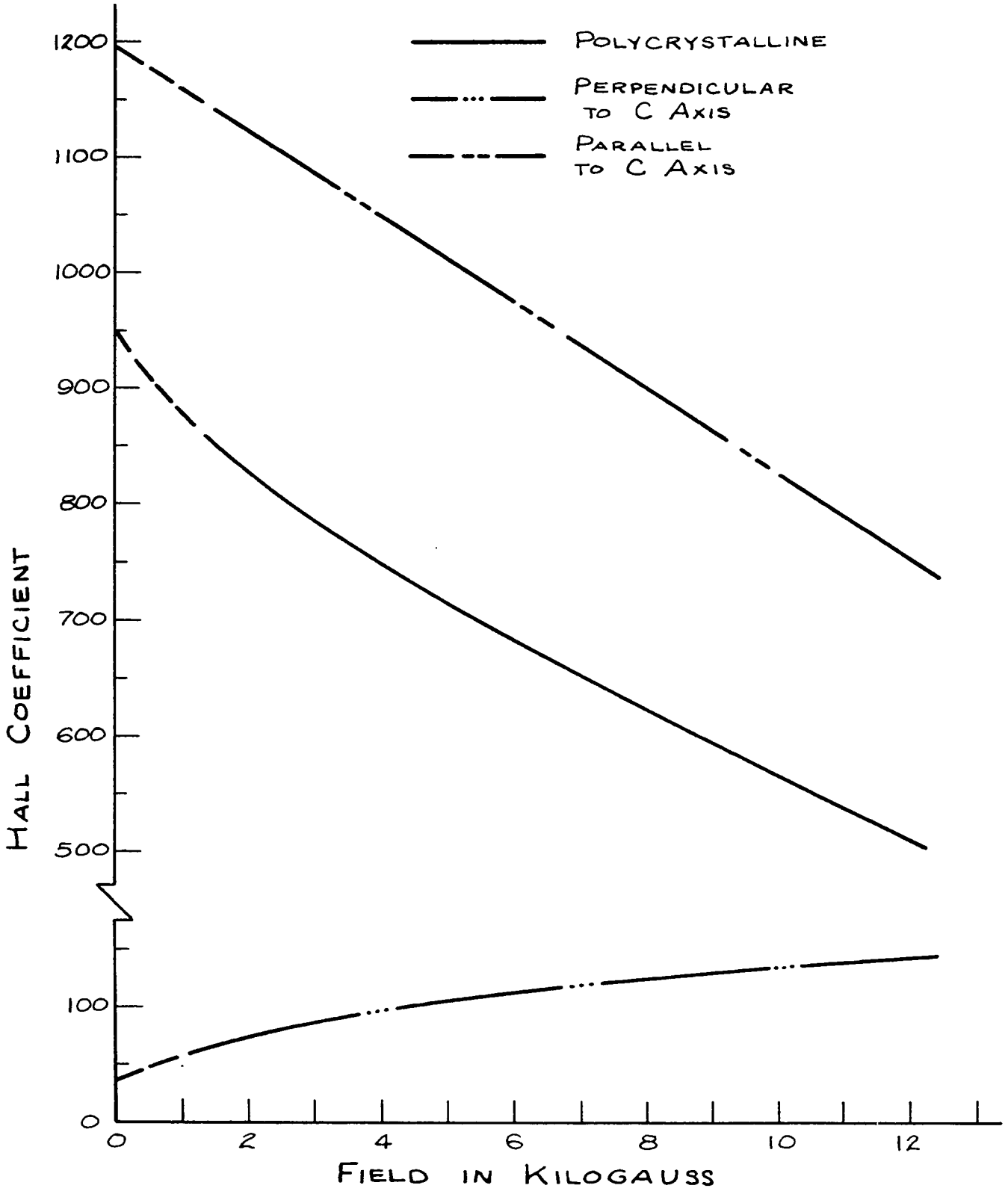
POLYCRYSTALLINE
PERPENDICULAR TO C AXIS
PARALLEL TO C AXIS
HALL COEFFICIENT
1200
1100
1000
900
800
700
600
500
100
0
0
2
4
6
8
10
12
FIELD IN KILOGAUSS

and then by a jeweler's saw which brought the dimensions to the approximate sizes of one-fourth by one by two and one-half inches and one-fourth by one by one and one-half inches. The specimens were then hand polished to the final size of 0.3 by 1.2 by 3.15 cm for the polycrystalline, 0.284 by 1.235 by 5.7 cm for the long dimension parallel to the c axis, and 0.3 by 1.23 by 3.15 cm for the long dimension perpendicular to the c axis. The crystals were then etched and again photographed with the Laue camera to check orientation and to ensure that the specimens were still single crystals.

C. Measurement of Hall Coefficient and Magneto Resistance

A specimen holder made from plexiglass allowed pressure contacts between pointed copper wire and the specimen which was positioned as illustrated in Figure 3. The Hall voltage was measured between probes A and B with the magneto resistance measured between probes B and C. To eliminate error in measurement due to possible nonalignment of probes A and B and contact potentials, the following procedure was used. Four readings were made for each magnetic field setting. The combination consisted of the current being reversed with the magnetic field constant. Then the magnetic field was reversed and readings repeated with the current flow in each direction. The results of these measurements are shown in Figures 4, 5, and 6.

D. Mounting of Specimens

Each specimen has lead-bismuth low temperature soldered attachments for current to be led to and from the specimen. Each specimen was drilled through the d dimension (Figure 3) with a number 76 drill to assure a tight fit for the copper probes. The specimen container included aluminum shields to help minimize convection heat transfer and a heater. The copper-constantan thermocouples were hand wound leaving a copper length of approximately 2 cm in length beyond the winding. This length was then inserted through the drilled hole. This was a tight fit, but, to assure that the wire would not pull out, it was bent to the side and then cut off near the surface of the specimen. It is noted here that the specimens were heated approximately 15^{o} C during irradiation, and, since bismuth contracts during heating, the holes became smaller affording a good contact. This type of instrumentation allowed measurement of temperature and temperature gradient as well as resistivity measurements.

E. The Electrical Circuit

Figure 7 shows a schematic drawing of the two systems used. The current source was two standard six volt auto batteries connected in parallel. The switch board connected to the potentiometer allowed rapid switching to facilitate measurement of potential drop across the standard resistor and the specimen.

Figure 7. Wiring diagram showing the instruments as used in the irradiation experiment

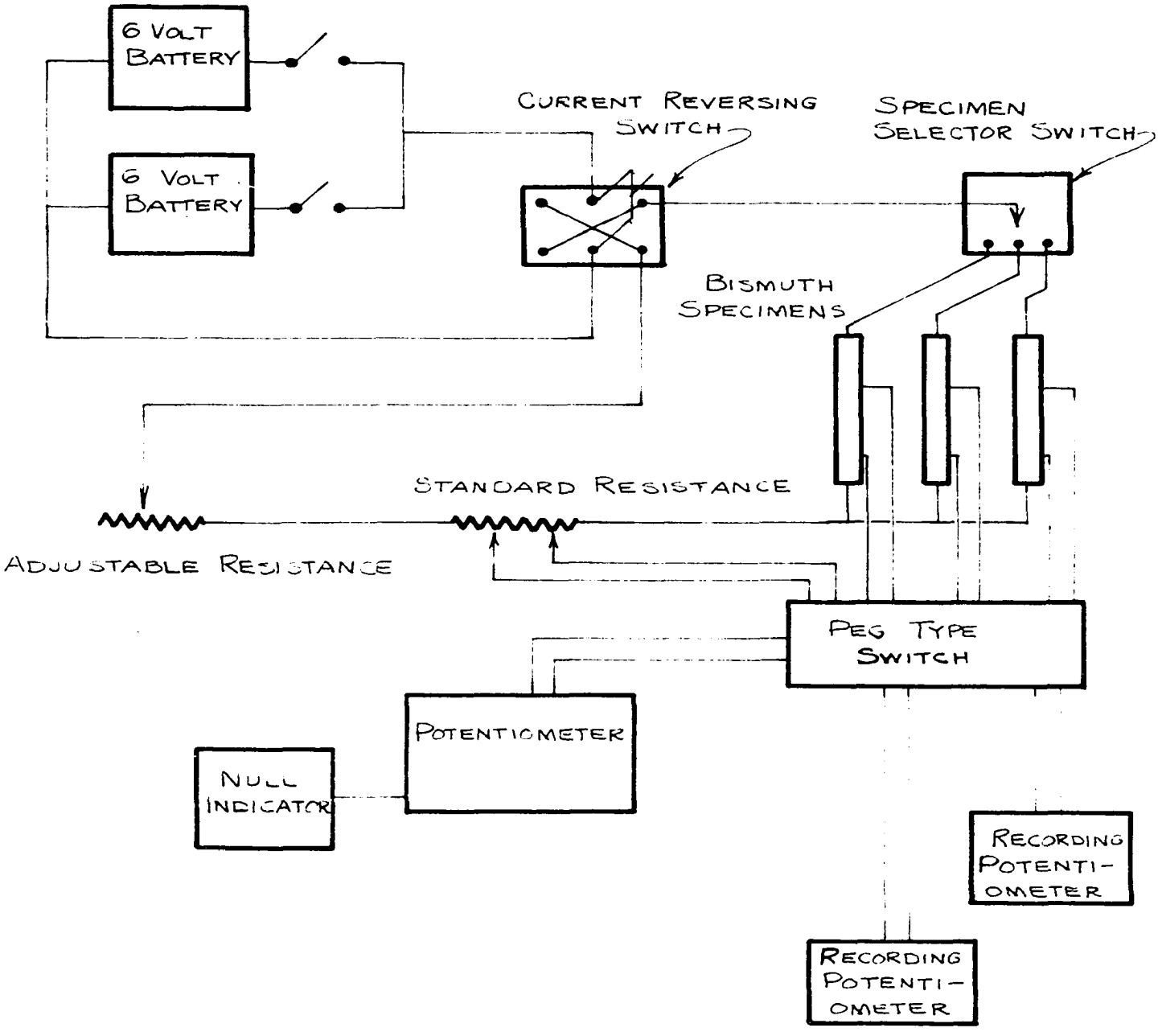
6 VOLT BATTERY
6 VOLT BATTERY
CURRENT REVERSING SWITCH
SPECIMEN SELECTOR SWITCH
BISMUTH SPECIMENS
STANDARD RESISTANCE
ADJUSTABLE RESISTANCE
PEG TYPE SWITCH
POTENTIOMETER
NULL INDICATOR
RECORDING POTENTI-OMETER
RECORDING POTENTI-OMETER

F. Measurement of Electrical Resistance

The procedure employed in measuring the potential drop across the specimen was set up to minimize errors in the final result. The reversal of the current was to prevent build up of a temperature gradient. The magnitude of the current was varied in each direction and then the resistance determined was plotted against current. Extrapolation to zero current gave a factor that would include effects of contacts, end corrections, etc. This procedure was necessary due to the large thermoelectric effects between copper and bismuth.

The thermocouples were calibrated for reading temperatures between 18^{o} C and 60^{o} C. Electrical resistivity curves as shown in Figure 11 were run for each specimen in the temperature range between 18^{o} C and 60^{o} C. These resistivity measurements were repeated in the reactor in the temperature range of 18^{o} C to 35^{o} C, the maximum attainable temperature from the heater in the reactor environment.

G. Reduction of Data

Figure 8 shows a graph of the irradiation data for all crystals. It should be noted that the time axis on the graph has three different scales. The appendix contains these data and an illustration of the step by step procedure for arriving at the final resistivity.

The electrical resistivity and current are listed in the first columns along with the time. The time runs from zero,

Figure 8. A graphical representation of the data obtained from the bismuth crystals

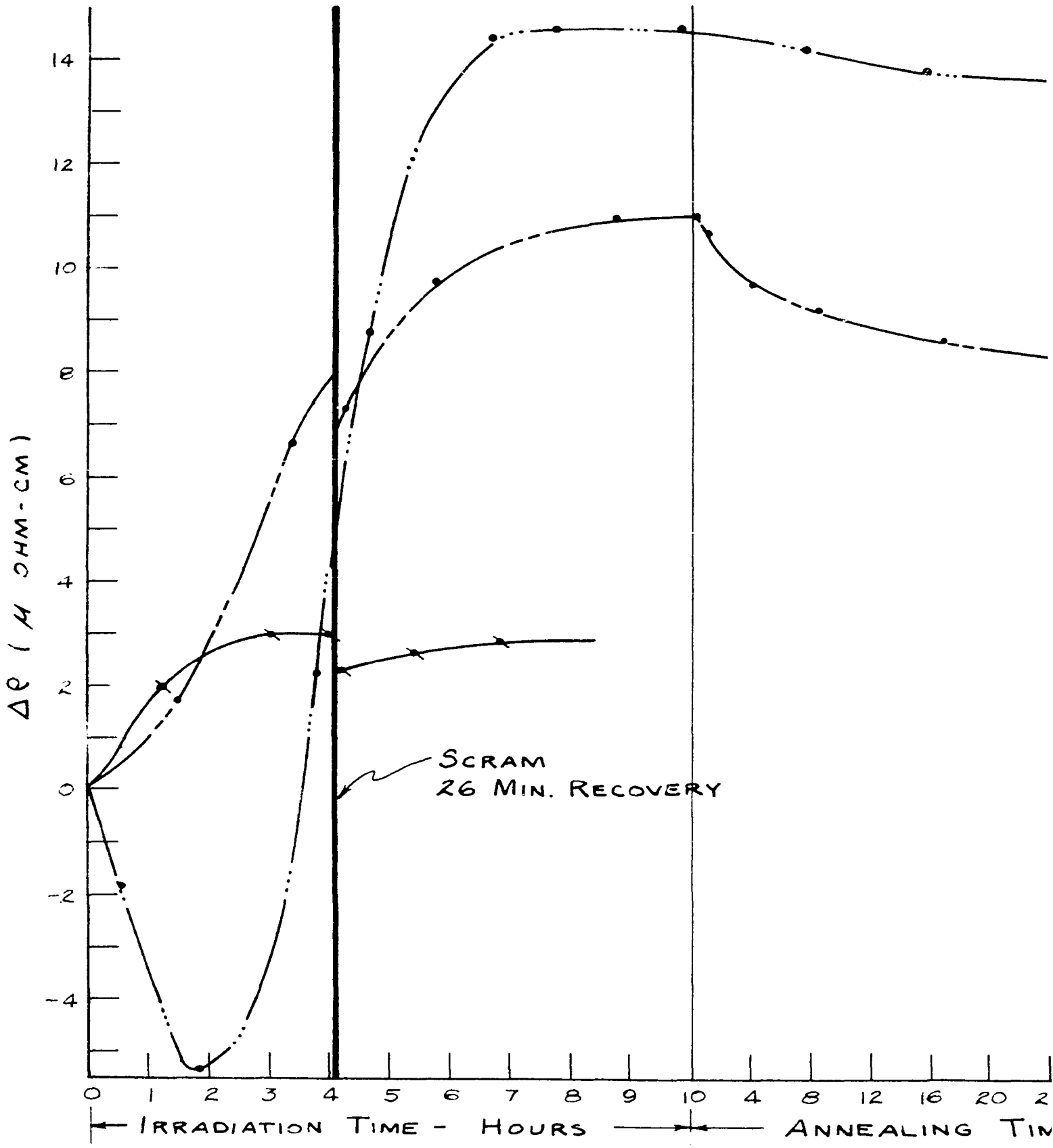
14
12
10
8
6
4
2
0
-2
-4
Δρ (μ OHM-CM)
SCRAM
26 MIN. RECOVERY
0 1 2 3 4 5 6 7 8 9 10 4 8 12 16 20
IRRADIATION TIME - HOURS
ANNEALING TIM

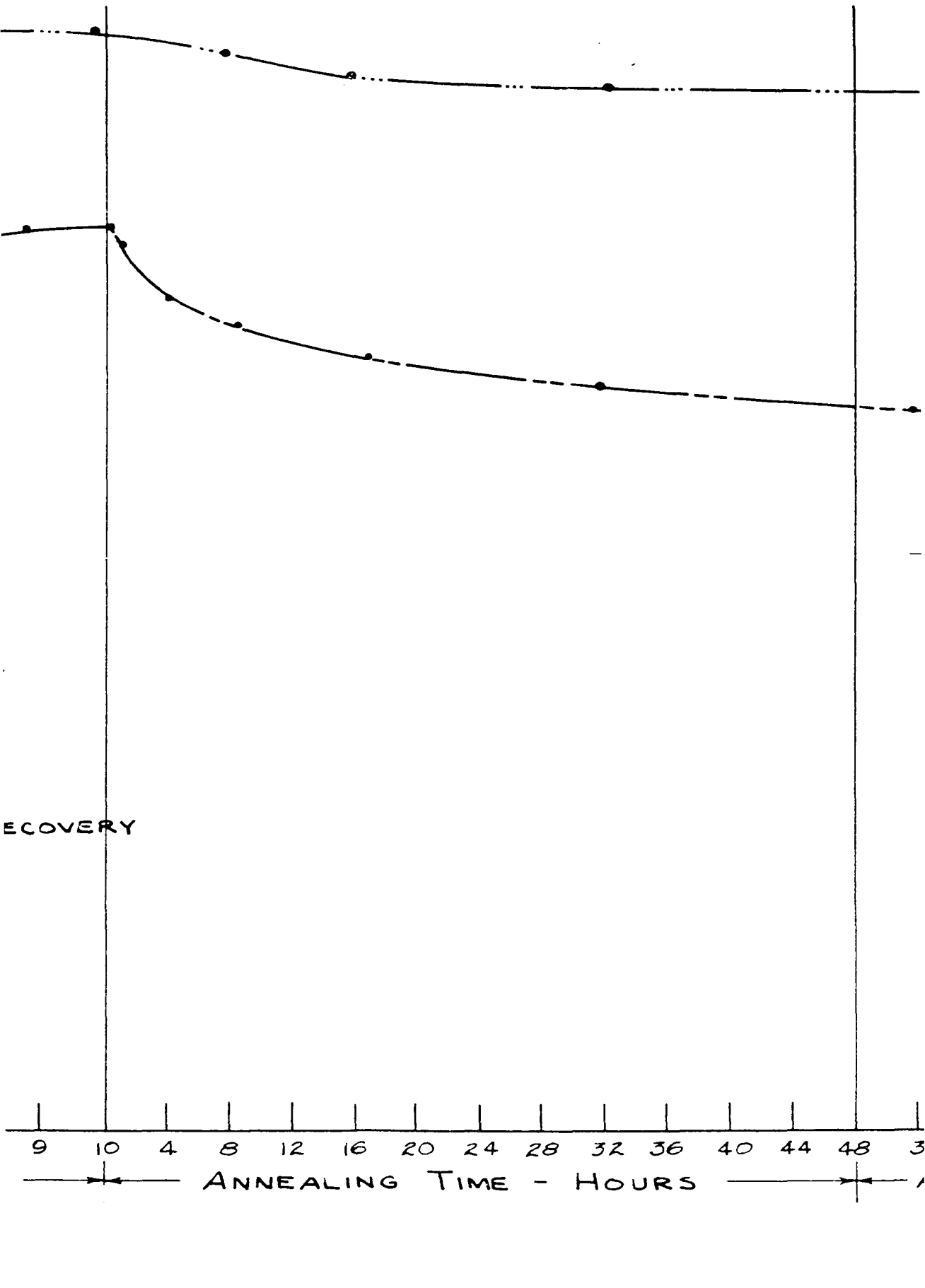
ECOVERY
9
10
4
8
12
16
20
24
28
32
36
40
44
48
ANNEALING TIME - HOURS

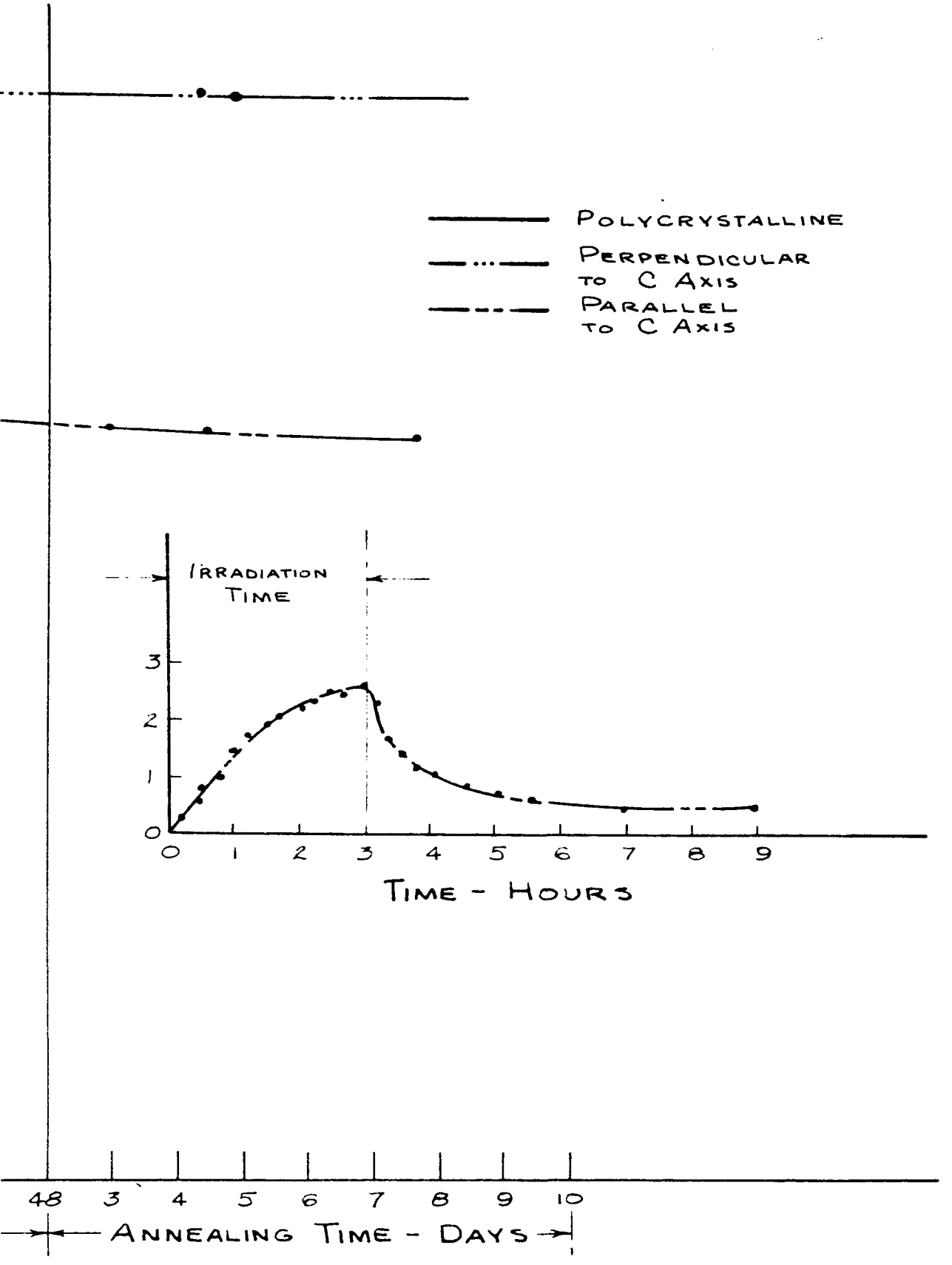
POLYCRYSTALLINE
PERPENDICULAR TO C AXIS
PARALLEL TO C AXIS
IRRADIATION TIME
0
1
2
3
0 1 2 3 4 5 6 7 8 9
TIME - HOURS
48 3 4 5 6 7 8 9 10
ANNEALING TIME - DAYS

the point at which the reactor reached the power level of 10 kw, until the reactor was shut down. The annealing time begins at this point. The temperature was monitored and is listed in the column after the measured resistivity. The next column lists the temperature correction applied to the resistivity. Since the annealing curve is of primary concern along with the equilibrium change in resistivity, this correction brings the resistivity for all measurements up to the temperature at which annealing began. The next column is the corrected resistivity, and it is the change in this value that is tabulated in the last column. This is the value plotted in Figure 8.

H. Measurement of the Flux Spectra

The flux spectra can be obtained approximately by utilizing indium foils covered with materials of known neutron absorption cross sections. The cross sections as presented by Hughes (21) were replotted on rectangular graph paper, and the area under each curve measured by means of a planimeter. Average cross sections for a specific energy range were then tabulated. Scattering cross sections were taken as a mean value and then subtracted leaving an approximate absorption cross section. Certain elements such as aluminum, manganese, and molybdenum have resonance absorption peaks in different energy ranges. When different combinations are used with cadmium as cover over indium, it could be assumed as a first

estimate that neutrons with their energies within the resonance ranges would be absorbed, and the activity of the indium would come from energy ranges not covered by the high absorption areas. It was found, however, that the slowing power of light elements such as aluminum is too great, and foils covered with aluminum and manganese combined with cadmium actually had a higher activity than the indium foils covered with cadmium alone. The molybdenum appeared to work well. Therefore, the following technique was used.

The combination of cadmium, indium, and molybdenum provided four equations containing activities caused by absorption of neutrons in the indium from nine energy ranges. These ranges were divided so that each contained a power of ten electron volts. For example, the first energy range was between .01 ev and 0.1 ev. The highest energy range was from 1 Mev to 10 Mev, and it is assumed that the number of neutrons above this are negligible. The activities corrected to the core center give the following relationships:

Indium foil bare:

$a + b + c + d + e + f + g + h + i = 10.4 \times 10^{11}$ disintegrate/sec

Cadmium covered indium:

$c + f + g + h + i = 1.912 \times 10^{11}$ disintegrate/sec

Subtracting above:

$a + b + d + e = 8.488 \times 10^{11}$ disintegrate/sec

Cadmium and molybdenum covered indium:

$$c + \qquad f \qquad = 1.9 \times 10^{11} \text{ disintegrate/sec.}$$

An approximate solution was found by using five by ten cycle log-log paper and plotting a bar graph, balancing the areas under each bar in the specific energy range so that the total area satisfied the four equations. Since the general shape of the curve is known, it is believed that the curve is a reasonable first estimate. More elaborate experiments are necessary to provide nine independent equations to give a better curve. Once the activity attributed to a specific energy region is known, the neutron flux can be calculated from the known activation cross sections and the number of atoms in the foil. The resulting flux spectra is approximated by the following relationships:

$$Q = 2.8 \times 10^{11} \qquad 0.01 \leq E \leq 1.0 \text{ ev}$$

$$Q = 10^{11} E^{-1.2} \qquad 1.0 \leq E \leq 10^{7} \text{ ev} \quad . \qquad (43)$$

V. INTERPRETATION OF DATA

A. Analysis of the Annealing Curve for the Crystal with Conduction along the C Axis

The data given in the appendix are presented in graphical form in Figure 8. Figures 9 and 10 present decay curves graphed on semilog paper for annealing at two different temperatures. It is seen that two distinct half lives are present in each instance. It is assumed that the short half life in each case represents the same type of annealing process. When this assumption is made and the ratio of the decay constants is found for each process, the rate constant and activation energy can be calculated. The procedure is as follows:

$$\lambda = K\, e^{-E/kT}$$

Process 1	Process 2
$0.1025 = K_1\, e^{-E_1/0.0265}$	$.047 = K_2\, e^{-E_2/.0265}$
$1.68 = K_1\, e^{-E_1/0.0281}$	$1.0 = K_2\, e^{-E_2/.0281}$
$0.061 = e^{-2.1\, E_1}$	$.047 = e^{-2.1\, E_2}$
$E_1 = 1.0$ ev	$E_2 = 1.46$ ev
$K_1 = 1.98 \times 10^{15}$	$K_2 = 2.44 \times 10^{22}$

The values obtained for E_1 and E_2 are somewhat lower than expected. Many semiconductors are believed to have about 2 ev as a mean value for the activation energy.

Figure 9. Annealing curve for the bismuth crystal with conduction parallel to the c axis (annealing temperature 38° C)

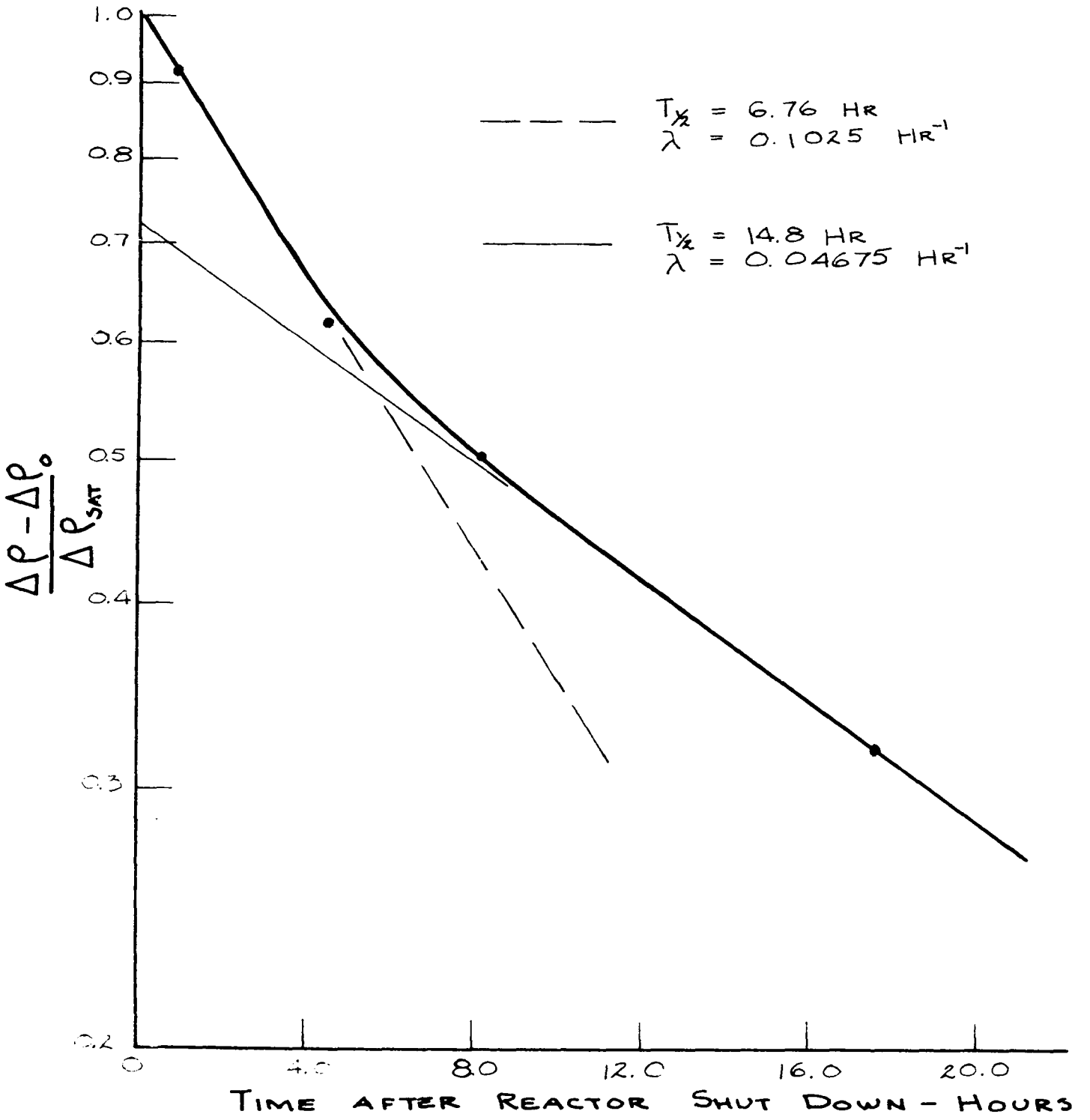
1.0
0.9
0.8
0.7
0.6
0.5
0.4
0.3
0.2
$\frac{\Delta P - \Delta P_0}{\Delta P_{SAT}}$
$T_{1/2}$ = 6.76 HR
λ = 0.1025 HR^{-1}
$T_{1/2}$ = 14.8 HR
λ = 0.04675 HR^{-1}
0
4.0
8.0
12.0
16.0
20.0
TIME AFTER REACTOR SHUT DOWN - HOURS

Figure 10. Annealing curve for the bismuth crystal with conduction parallel to the c axis (annealing temperature 56.5° C)

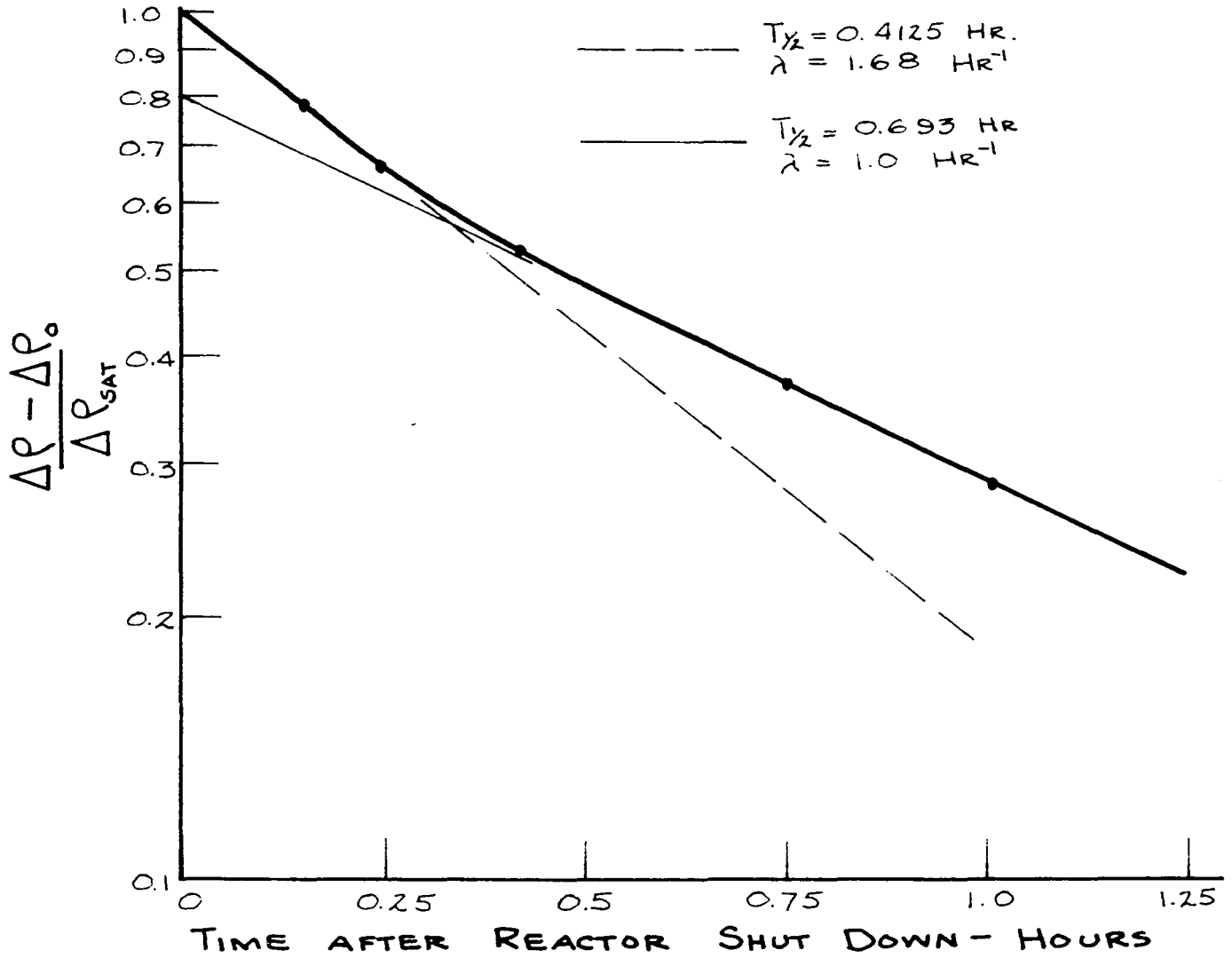
1.0
0.9
0.8
0.7
0.6
0.5
0.4
0.3
0.2
0.1
$\frac{\Delta P - \Delta P_o}{\Delta P_{SAT}}$
$T_{1/2} = 0.4125$ HR.
$\lambda = 1.68$ HR^{-1}
$T_{1/2} = 0.693$ HR
$\lambda = 1.0$ HR^{-1}
0
0.25
0.5
0.75
1.0
1.25
TIME AFTER REACTOR SHUT DOWN - HOURS

The value of the rate constant for K_2 is high. The literature states that the mean value for the rate constant lies between 10^8 and 10^{18}, the high end applicable primarily to semiconductors.

The literature revealed that the activation energy for interstitials for all materials discussed is less than that required for vacancies. This indicates that the short half life activity is probably due to the annealing of the interstitial atoms. A supporting argument concerns the contribution to the total change in resistivity during equilibrium. Of the total resistivity change, 11 μ ohm-cm, only 3.6 μ ohm-cm annealed in the time indicated on the graph in Figure 8. Using this as the total change due to annealing, Figure 9 can be interpreted to read that 28 percent of this total change or 1.01 μ ohm-cm of resistance is attributed to the process with the short half life. The other process accounts for 2.59 μ ohm-cm resistivity change.

The comparison of the relative effects of interstitial atoms and vacant lattice sites on the resistivity given in equation 40 can now be used to help estimate the number of interstitial atoms and vacant lattice sites. This relationship estimated that an interstitial atom had 4.5 times the effect on electrical resistivity as did a vacant lattice site. Let the subscript 1 refer to the vacant lattice site and the subscript 2 refer to the interstitial atom. The relationships

for the equilibrium condition under irradiation can be written

$$P_1 = \lambda_1 N_1$$

$$P_2 = \lambda_2 N_2 \quad . \quad 44$$

The data reduce to the value

$$\frac{\Delta \varrho_1}{\Delta \varrho_2} = 2.57 \quad . \quad 45$$

Using the theoretical value of 4.5 as the relative effect of the two types of impurities and equation 45 produces the equilibrium relationship

$$N_1 = 11.6\ N_2 \quad . \quad 46$$

Substituting equation 46 and the experimental values for λ_1 and λ_2 into equation 44 reveals that for the equilibrium production rate

$$P_1 = 0.71\ P_2 \quad . \quad 47$$

This relationship reveals that the production rate of vacancies is only 71 percent as great as that for interstitial atom formation. This difference from a one to one production rate may be attributed to the contribution from the displacement spike.

Equation 18 indicated that approximately 1.47×10^{14} pairs of interstitial atom and vacancy lattice sites are produced per second via the thermal spike. When this is substituted into the equilibrium relationship, there results a value for the number of vacant lattice sites per cm^3. This number is 5.16×10^{18}. The number of interstitials is found

from equation 46 and is 4.45×10^{17} atoms per cm^3.

There was a 7.4 μ ohm-cm resistivity which did not anneal. This resistance cannot be attributed to any one type of impurity. At any temperature there is a saturation concentration of vacancies and interstitials that can be supported in a crystal without annealing taking place. In bismuth this allowed concentration decreases as the temperature increased. Therefore, the crystals can be assumed to have absorbed the damage caused by the neutrons until the saturation point. Then the number produced above this point came into equilibrium with the annealing rate.

In equation 3 it was stated that during the equilibrium phase of the irradiation it was possible to write $\Delta\rho = B\,N$. The values given above result in

$$B_1 = 4.42 \times 10^{-19} \left(\frac{\mu_{\text{ohm-cm}^4}}{\#\ \text{vacancies}} \right)$$

$$B_2 = 2.27 \times 10^{-18} \left(\frac{\mu_{\text{ohm-cm}}}{\#\ \text{vacancies/cm3}} \right)$$

B. Analysis of the Data Received from the Specimen with Conduction Perpendicular to the C Axis

The graph of the data reveals that this crystal initially had a decrease in electrical resistivity followed by a sharp increase, reaching a saturation point in less time than that required for the $\rho_{\parallel}$ specimen. After reactor shut down, this crystal did not anneal to the extent as did the $\rho_{\parallel}$ crystal.

In this crystal only a very small amount of annealing occurred. This makes it difficult to analyze the decay curve in the same manner as used for the $\rho_{\parallel}$ crystal.

However, it can be seen that the short half life decay process did not contribute to the part that did anneal in any significant manner. This means that the interstitial atom density above the equilibrium level was very low. On the other hand, the vacant lattice sites were also less dense.

There are several reasons that this type of annealing curve was found. First, there is the possibility that the flux may have been lower at this location since the thermocouple leads from the other two crystals passed by this crystal. However, the masses involved make this seem unlikely. The second and most plausible reason concerns the effect of the electron current on the impurities caused by irradiation. This crystal presents planes of atoms perpendicular to the electron current flow. The structure will have two planes close together, then a larger dimension before the next two planes. An interstitial atom must sit between these planes, and has the highest probability of being found between planes that are the farthest apart. The activation energy will be the greatest for interstitial atoms located between the planes lying closest together. It is conceivable, therefore, that the forces involved in the interaction between the electrons and lattice strains may have caused the interstitial

atoms with the lower activation energy to anneal more rapidly. The few that remained, along with the vacant lattice sites, could have been adequate to give the equilibrium level for the change in resistivity during irradiation.

The literature points out that in some semiconductors the resistivity change follows a curve similar to that presented here, that is, a sudden drop and then a sudden recovery. Some semiconductors do just the reverse. The explanation normally given refers to the Fermi surface and the width of the forbidden zone in the band theory. As has been previously mentioned, bismuth has a very small energy gap. Therefore, the sudden introduction of a high neutron flux environment may tend to lower the Fermi energy and to therefore put more carriers into the system. Reference 22 gives data showing this to be true in semiconductors. It does not take long for the saturation point to be reached at which point the increase in carriers is offset by the radiation damage shortening the carrier relaxation length.

It is also possible that initially the irradiation environment was annealing the work hardening and other residual stresses set up in the specimen. Figure 3 illustrates slip lines that were visible on the crystal surface which indicate some atomic movement had taken place. However, all crystals were handled in the same fashion and such a curve did not occur in either the polycrystalline or the $\rho_{\parallel}$ specimen.

It is also noteworthy that at this minimum in resistivity the overall value was still much higher than for $\rho_{\parallel}$. This shows that the extra carriers introduced were not sufficient in number to be noticeable in the $\rho_{\parallel}$ specimen. The magneto resistance and Hall coefficients shown in Figures 4, 5, and 6 show that the effective carrier relaxation time for $\rho_{\perp}$ is much greater than for the $\rho_{\parallel}$ specimen.

C. Analysis of Data from the Polycrystalline Specimen

The data from the polycrystalline specimen shown plotted in Figure 8 is difficult to analyze. At first glance one might suspect that the $\Delta\rho$ curve should look something like a compromise between the curves for the single crystal data, particularly when one considers that the average in bismuth is $\bar{\rho} = 1/3\,\rho_{\parallel} + 2/3\,\rho_{\perp}$. Note that this fits the preirradiation data very well. However, the literature has shown that the overall picture is not as simple as this. To explain data on polycrystalline samples, new theories are currently being tested. These theories are concerned with the mechanism of annealing. Many people are now of the opinion, for example see reference 23, that the impurities initially form pairs, then larger clusters, and finally some anneal on the crystal surface. The data from this specimen appear to indicate that this is the case for bismuth. The twenty six minute delay when the reactor inadvertently scrammed helps strengthen this point. It appears that of the damage accumulated about thirty

percent of it annealed during this time. This is not the case for either of the single crystals.

These data point to a method which may help establish the theory concerned with defects clustering and annealing on a crystal surface. If annealing occurs in this manner, it should be possible to plot a curve of the rate constant for a specific type defect against crystal surface area density. The crystal surface area density would depend on the size of the crystals. The single crystal could be assumed to present a zero value for this density. Several polycrystalline specimens of known uniform crystal size, with sizes varying from one crystal to another, subjected to a similar environment as the single crystal should give sufficient data to plot the curve. The slope of this curve would be an indication of the rate constant dependence upon the surface area. If the slope is zero, it could be concluded that the surface area has no effect. However, the polycrystalline specimen tested here indicates that the slope would not be zero.

VI. DISCUSSION

The analysis as described in this thesis shows a method that makes it possible to obtain some agreement between the theory of irradiation damage and experimental data. The normal, or generally accepted, manner of reporting irradiation dose rate must be supplemented with additional information before comparison can be made. The nvt magnitude along with temperature is entirely inadequate without a statement of the flux spectra. It also appears that the polycrystalline material data must include reasonably accurate estimates of the crystal size. Included in the above must, of course, be the most accurate data available concerning impurity concentrations.

The procedure established for this thesis reveals that it is possible to separate the effects of the various impurities on the electrical resistivity. With this information available, it is then possible to make an additional check on theoretical calculations, and to determine more accurately where the theoretical errors lie. When this theoretical value for the effect on resistivity of various impurities is known, it is possible to determine accurately the proportionality constant between impurity concentration and electrical resistivity. The final link in the theory will be a check on the impurity production rate.

This thesis shows an approach which may help in corre-

lating experimental data. To facilitate this correlation, it is desirable to replace the integrated flux with an effective flux corrected to eliminate the annealing rate.

The accuracy of the data presented here depends primarily upon the errors inherent in measuring physical properties of matter and upon corrections for temperature variation. Reversal of the current eliminated consideration of the build up of surface potentials. The accuracy of the recording equipment would allow the introduction of errors ranging from one to five percent in the reading. However, pre-irradiation tests, using the same method as was employed throughout the experiment, agreed well with published results of other experimenters. The correction factor which corrected the resistance to zero current was considered constant throughout the irradiation experiment. A number of checks were made to verify this assumption. These tests confirmed that the factor remained constant.

The effect of the temperature variation can only be estimated. All corrections were made from curves appearing in the appendix. These curves represent the resistivity for the bismuth before irradiation. How correct these curves are for bismuth during irradiation is not known. When one analyzes the problem and takes into consideration that the temperature only changes a few degrees the error introduced

here should not be great. This means that the data should be consistent within itself with errors perhaps in the order of one percent.

VII. CONCLUSIONS

> "The major problems in the theory of radiation effects may be classified in three categories: (1) the mechanism of damage production, (2) the nature and mobility of the imperfections produced, and (3) the effect of imperfections on measurable properties of the solid. It is difficult to make a clear separation of these areas since, for example, the answer to (2) depends greatly on (1) and (3) provides the only experimental means of studying (1) and (2)." - Brooks (5).

1. The half life approach has provided a means of determining the relative effects of the individual types of irradiation damage on the resistivity. This approach is a solution of (3) and, therefore, allows reactor study of (1) and (2).
2. The half life approach provides a basis for an experimental procedure to determine the proportionality constant between electrical resistivity and the concentrations of a particular type of defect.
3. This half life approach provides a more direct method than the temperature variation method of determining activation energy for a specific type impurity.
4. The annealing activation energy in bismuth for interstitials is 1 ev and for vacant lattice sites is 1.46 ev, limited, of course, by the accuracy of the data.
5. The half life approach introduced here provides a means of correlating experimental data with theoretical calculations of the effects of the individual radiation produced impurities on the electrical resistivity.

VIII. SUMMARY

The quantity of irradiation damage in solids can be estimated from electrical resistivity measurements during and after irradiation. For low neutron flux irradiation experiments at room temperature, the damage rate in bismuth will reach an equilibrium balance with the annealing rate. This fact points out the fallacy of giving radiation dosages in nvt along with the irradiation temperature. The annealing curve for the change in resistivity after reactor shut down can be analyzed to determine the types of impurities which are annealing and their activation energy. In bismuth it was found that the interstitial atoms annealed with an activation energy equal to 1 ev while the vacant lattice sites annealed with an activation energy equal to 1.46 ev.

The theoretically derived relationship between the effect of one percent interstitial atoms and one percent vacant lattice sites indicated that the interstitial atom has 4.5 times as great an effect on the electrical resistivity as does a vacant lattice site. This value and the relative amounts of change in electrical resistivity during the equilibrium balance between production and annealing allowed an estimate which revealed the relative concentrations of interstitial atoms and vacant lattice sites. It was found that there were 11.61 times as many vacant lattice sites as interstitial atoms, and that the relative production rate of vacancies was only 71 percent as great as that for interstitial atoms. With a production rate calculated

from some approximate information such as the flux spectra, this indicates a concentration of 5×10^{18} vacancies and 4×10^{17} interstitial atoms per cm^3 during equilibrium. This means there were approximately 0.02 percent vacancies and 0.002 percent interstitial atoms.

The data from the irradiated specimens show that the polycrystalline sample annealed the damage at a much higher rate than either of the single crystals. This indicates that the migration of the impurities may have been to the grain boundaries.

IX. BIBLIOGRAPHY

1. Seitz, Frederick and Koehler, J. S. Displacement of atoms during irradiation. In Seitz, Frederick and Turnbull, David, eds. Solid state physics. Vol. 2. pp. 305-448. New York, N. Y., Academic Press Inc. 1956.

2. Wilson, A. H. The theory of metals. 2nd ed. London, Eng., Cambridge at the University Press. 1958.

3. Kinchin, G. H. and Pease, R. S. The displacement of atoms in solids by radiation. Rept. Prog. in Physics 18:1. 1955.

4. Dienes, G. J. and Vineyard, G. H. Radiation effects in solids. Interscience Monographs in Physics and Astronomy. Vol. 2. 1957.

5. Brooks, Harvey. Radiation effects in materials. Journal of Applied Physics 30:1118. 1959.

6. Bohr, N. The penetration of atomic particles through matter. Kgl. Danske Videnskab. Selskab, Mat. - fys. Medd. 18:8. 1948.

7. Snyder, W. S. and Neufeld, J. Disordering of solids by neutron irradiation. Phys. Rev. 97:1635. 1955.

8a. Huntington, H. B. Mobility of interstitial atoms in a face-centered metal. Phys. Rev. 91:1092. 1953.

8b. _____ . Creation of displacements in radiation damage. Phys. Rev. 93:1414. 1954.

9. Seitz, Frederick. The disordering of solids by action of fast massive particles. Discussions of Faraday Society 5:271. 1949.

10. Brinkman, J. A. On the nature of radiation damage in metals. Journal of Applied Physics 25:961. 1954.

11. Blewitt, T. H., Coltman, R. R., Holmes, D. K. and Naggle, T. S. Mechanism of annealing in neutron irradiated metals. Unpublished ORNL-2188 (Oak Ridge National Lab.)

12. Charlesby, A. Atomic radiation and polymers. London, Eng., Pergamon Press Ltd. 1960.

13. Mott, N. F. and Jones, H. The theory of the properties of metals and alloys. New York, N. Y., Dover Publications Inc. 1936.

14. Blatt, F. J. Effect of point imperfections on the electrical properties of copper: I. Conductivity. Phys. Rev. 99:1708. 1955.

15. Overhauser, A. W. and Gormann, R. L. Resistivity of interstitial atoms and vacancies in copper. Phys. Rev. 102:676. 1956.

16. Rubenstein, R. A. Theoretical study of the auger effect in the light to medium range of atomic number. Unpublished Ph. D. Thesis. Urbana, Illinois, University of Illinois Library. 1955.

17. Aschner, J. F. Self-diffusion in sodium and potassium chloride. Unpublished Thesis. Urbana, Illinois, University of Illinois Library. 1954.

18. Fuchs, K. A quantum mechanical calculation of the elastic constants of monovalent metals. Proc. Roy. Soc. of London Series A, 153:622. 1936.

19. Huntington, H. B. and Seitz, Frederick. Mechanism for self-diffusion in metallic copper. Phys. Rev. 61:315. 1942.

20. Bohm, D. Quantum theory. Englewood, N. J., Prentice-Hall Inc. 1951.

21. Hughes, D. J. Neutron cross sections. BNL-325 (Brookhaven National Lab.). 1960.

22. Sonder, E. Magnetic and electrical properties of reactor irradiated silicon. Journal of Applied Physics 30:1186. 1959.

23. Wertheim, G. K. Recombination properties of bombardment defects in semiconductors. Journal of Applied Physics 30:1166. 1959.

X. ACKNOWLEDGMENTS

In the course of completing this dissertation the author has incurred the debt of gratitude to members of the Iowa State University staff.

It is a pleasure to express a large debt of gratitude to Dr. Glenn Murphy, Professor and Head of the Department of Nuclear Engineering at Iowa State University, who, as major professor and teacher, has aided the author immeasurably during the past three years.

The author also wishes to acknowledge the help of Dr. Arthur Pohm of the Electrical Engineering Department of Iowa State University and Mr. Paul Sidles of the Institute for Atomic Research who through many discussions aided the author in the understanding of the theoretical and experimental techniques involved in this thesis.

XI. APPENDIX

Table 1. Electrical resistivity data from the polycrystalline specimen (correction factor to zero current is 0.902)

Time (hours)	Volt drop across std. res.	Current flow (amps.)	Volt drop across specimen (μ-volt)	Resistance R = E/I (μ-volt)
0	.07764	2.725	1520	557
1.25	.07506	2.640	1512	573
3.0	.07830	2.750	1605	584
3.9	.07714	2.714	1595	588
4.2	.07845	2.760	1622	588
5.4	.07686	2.704	1610	594
6.8	.07784	2.739	1630	597

Table 1. (Continued)

Time (hours)	Resistivity (μ-ohm-cm) ρ	Temperature (^{o}C)	Resistivity correction to 38^{o}C	Corrected resistivity (μ-ohm-cm) ρ	$\Delta\rho$
0	120.8	22.0	6.7	127.5	0
1.25	124.0	25.0	5.5	129.5	2.0
3.0	126.1	28.0	4.4	130.5	3.0
3.9	127.1	30.2	3.4	130.5	3.0
4.2	127.0	31.0	2.8	129.8	2.3
5.4	128.7	35.0	1.4	130.1	2.6
6.8	129.3	36.0	1.0	130.3	2.8

Table 2. Electrical resistivity data from the specimen with conduction perpendicular to the c axis (correction factor to zero current is 0.948)

Time (hours)	Volt drop across std. res.	Current flow (amps.)	Volt drop across specimen (μ-volt)	Resistance R = E/I (μ-volt)
0	.08257	2.9050	1631	562
0.5	.08081	2.8434	1580	556
1.8	.08344	2.9359	1592	544
3.8	.08359	2.9414	1698	576
4.7	.08371	2.9456	1782	605
6.8	.08352	2.9388	1860	634
7.8	.08363	2.9508	1880	637
9.9	.08345	2.9363	1872	639
8.0	.08244	2.9010	1810	624
12.0	.08280	2.9130	1802	619
32.8	.08339	2.9347	1810	618
4.4 days	.08374	2.9462	1820	618
5.0 days	.08371	2.9454	1818	618
7.8 days	.08359	2.9414	1818	618

Table 2. (Continued)

Time (hours)	Resistivity (μ-ohm-cm) ρ	Temperature (^{o}C)	Resistivity correction to 38^{o}C	Corrected resistivity (μ-ohm-cm) ρ	$\Delta\rho$
0	135.2	22.0	3.8	139.0	0
0.5	133.7	23.0	3.5	137.2	-1.8
1.8	130.8	26.5	2.8	133.6	-5.4
3.8	138.8	30.0	2.5	141.3	2.3
4.7	145.8	32.0	2.0	147.8	8.8
6.8	152.4	36.0	1.0	153.4	14.4
7.8	153.0	37.0	0.6	153.6	14.6
9.9	153.6	38.0	0.0	153.6	14.6
8.0	150.2	24.8	3.0	153.2	14.2
12.0	149.0	22.2	3.8	152.8	13.8
32.8	148.7	22.0	3.8	152.5	13.5
4.4 d	148.7	22.0	3.8	152.5	13.5
5.0 d	148.7	22.2	3.8	152.4	13.4
7.8 d	148.7	22.2	3.8	152.5	13.5

Table 3. Electrical resistivity data from the specimen with conduction parallel to the c axis (correction factor to zero current is 0.97)

Time (hours)	Volt drop across std. res.	Current flow (amps.)	Volt drop across specimen (μ-volt)	Resistance R = E/I (μ-volt)
0	.08081	2.8434	3288	1138
1.5	.08045	2.8306	3305	1169
3.4	.08129	2.8604	3560	1242
4.3	.08175	2.87632	3622	1262
5.8	.08164	2.8727	3790	1320
7.3	.08204	2.9021	3835	1235
8.8	.08210	2.8890	3880	1341
10.1	.08210	2.8889	3870	1339
1.0	.08210	2.8890	3860	1338
4.3	.08165	2.8727	3810	1322
8.8	.08175	2.8763	3640	1268
17.0	.08205	2.8876	3550	1230
32.0	.08210	2.8884	3539	1225
3 days	.08210	2.8884	3528	1222
4.5 days	.08210	2.8884	3525	1221
7.7 days	.08206	2.8879	3525	1221

Table 3. (Continued)

Time (hours)	Resistivity (μ-ohm-cm) ρ	Temperature (^{o}C)	Resistivity correction to 38^{o}C	Corrected resistivity (μ-ohm-cm) ρ	$\Delta\rho$
0	110.7	22.0	8.5	119.2	0
1.5	113.4	26.0	7.5	120.9	1.7
3.4	120.8	29.5	5.0	125.8	6.6
4.3	122.5	31.0	4.0	126.5	7.3
5.8	128.0	36.0	1.0	129.0	9.8
7.3	128.8	36.0	1.0	129.8	10.6
8.8	130.2	37.5	0	130.2	11.0
10.1	130.1	38.0	0	130.1	10.9
1.0	129.9	37.9	0	129.9	10.7
4.3	128.4	36.5	0.5	128.9	9.7
8.8	122.9	24.0	5.5	128.4	9.2
17.0	119.3	22.0	8.5	127.8	8.6
32.0	118.7	22.0	8.5	127.2	8.0
3 days	118.3	22.0	8.5	126.8	7.6
4.5 days	118.2	22.0	8.5	126.7	7.5
7.7 days	118.2	22.0	8.5	126.7	7.5

Table 4. Electrical resistivity data from the specimen with conduction parallel to the c axis (correction factor to zero current is 0.97)

Time (hours)	Volt drop across std. res.	Current flow (amps.)	Volt drop across specimen (μ-volt)	Resistance R = E/I (μ-volt)
0	.0711	2.500	2985	1196
0.20	.0709	2.490	2990	1201
0.45	.0707	2.485	3002	1208
0.50	.0707	2.485	3020	1212
0.75	.0707	2.485	3018	1210
1.00	.0704	2.474	3010	1215
1.20	.0706	2.482	3050	1238
1.55	.0706	2.482	3160	1272
1.70	.0706	2.482	3180	1280
2.10	.0806	2.482	3230	1304
2.25	.0705	2.478	3250	1316
2.50	.0703	2.471	3310	1340
2.70	.0705	2.478	3350	1355
3.00	.0706	2.482	3370	1368
0.15	.0705	2.478	3360	1365
0.25	.0705	2.478	3350	1355
0.50	.0706	2.482	3355	1350
0.75	.0706	2.482	3342	1348
1.00	.0708	2.488	3350	1348
1.50	.0710	2.492	3350	1345
2.00	.0715	2.515	3350	1335
2.50	.0700	2.460	3260	1322
4.00	.0704	2.475	3190	1290
6.00	.0704	2.475	3150	1273

Table 4. (Continued)

Time (hours)	Resistivity (μ-ohm-cm) ρ	Temperature (^{o}C)	Resistivity correction to 56.5^{o} C	Corrected resistivity (μ-ohm-cm) ρ	$\Delta\rho$
0	116.00	22.0	14.0	130.00	0.00
0.20	116.50	22.2	13.8	130.30	0.30
0.45	117.10	22.4	13.5	130.60	0.60
0.50	117.50	22.6	13.3	130.80	0.80
0.75	117.90	23.4	13.1	131.00	1.00
1.00	118.60	25.0	12.8	131.40	1.40
1.20	120.20	28.0	11.5	131.75	1.75
1.55	123.50	33.0	9.5	132.00	2.00
1.70	124.10	36.0	8.0	132.10	2.10
2.10	126.75	43.0	5.5	132.25	2.25
2.25	127.80	45.5	4.5	132.30	2.30
2.50	130.00	50.0	2.5	132.50	2.50
2.70	131.45	53.0	1.0	132.45	2.45
3.00	132.60	56.5	0.0	132.60	2.60
0.15	132.30	56.6	0.0	132.30	2.30
0.25	131.80	56.7	0.0	131.80	1.80
0.50	131.45	56.7	0.0	131.45	1.45
0.75	131.20	56.5	0.0	131.20	1.20
1.00	131.05	56.3	0.0	131.05	1.05
1.50	130.35	54.6	0.5	130.85	0.85
2.00	129.15	52.0	1.6	130.75	0.75
2.50	128.05	49.5	2.6	130.65	0.65
4.00	125.05	43.8	5.4	130.45	0.45
6.00	123.50	38.5	7.0	130.50	0.50

Figure 11. Electrical resistivity of bismuth specimens

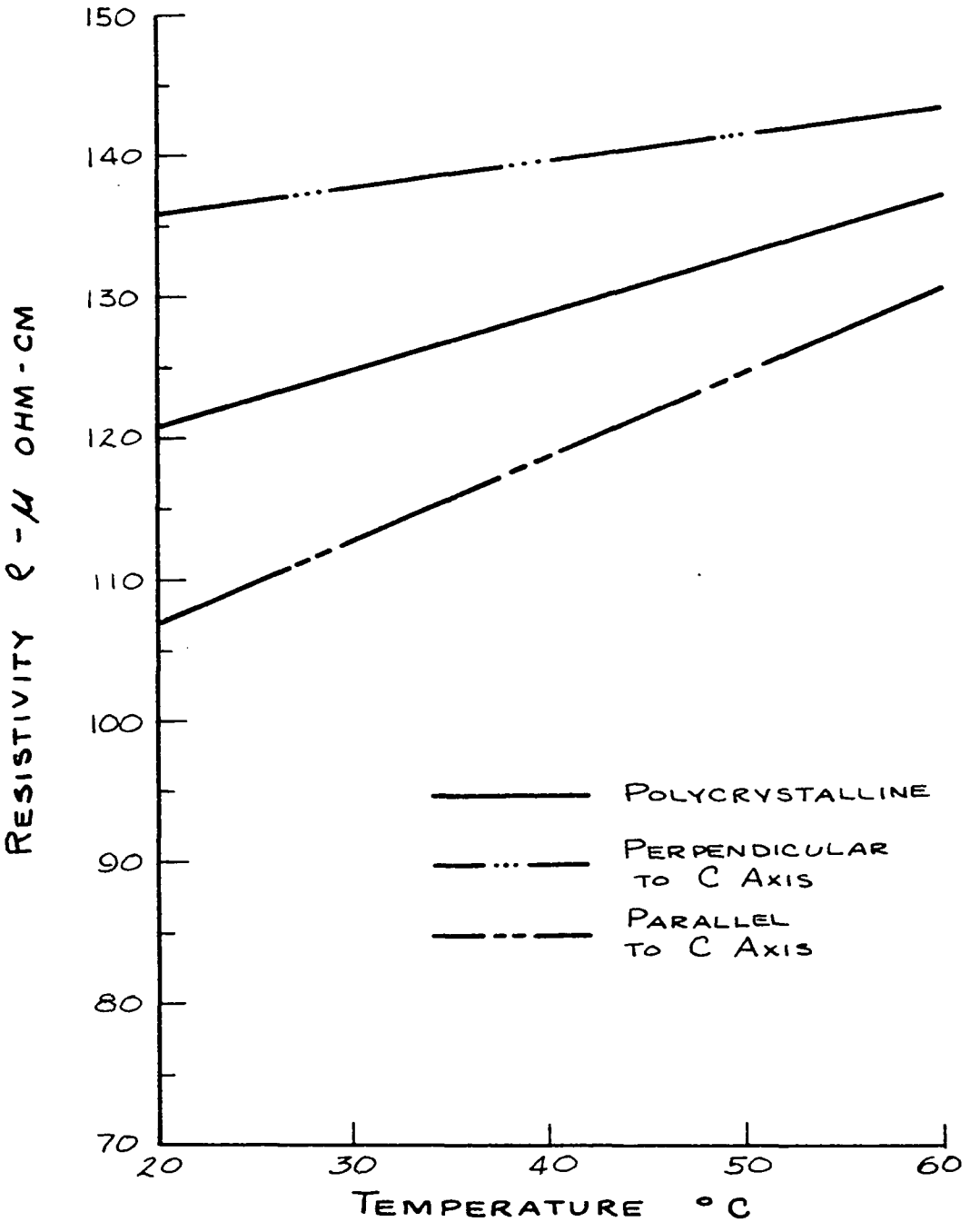
150
140
130
120
110
100
90
80
70
RESISTIVITY ρ - μ OHM - CM
20
30
40
50
60
TEMPERATURE °C
POLYCRYSTALLINE
PERPENDICULAR TO C AXIS
PARALLEL TO C AXIS